



# Role of continental recycling in intraseasonal variations of continental moisture as deduced from model simulations and water vapor isotopic measurements

Camille Risi, D. Noone, C. Frankenberg, J. Worden

## ► To cite this version:

Camille Risi, D. Noone, C. Frankenberg, J. Worden. Role of continental recycling in intraseasonal variations of continental moisture as deduced from model simulations and water vapor isotopic measurements. *Water Resources Research*, 2013, 49 (7), pp.4136-4156. 10.1002/wrcr.20312 . hal-01099540

**HAL Id: hal-01099540**

**<https://hal.science/hal-01099540>**

Submitted on 14 Jan 2015

**HAL** is a multi-disciplinary open access archive for the deposit and dissemination of scientific research documents, whether they are published or not. The documents may come from teaching and research institutions in France or abroad, or from public or private research centers.

L'archive ouverte pluridisciplinaire **HAL**, est destinée au dépôt et à la diffusion de documents scientifiques de niveau recherche, publiés ou non, émanant des établissements d'enseignement et de recherche français ou étrangers, des laboratoires publics ou privés.

# Role of continental recycling in intraseasonal variations of continental moisture as deduced from model simulations and water vapor isotopic measurements

Camille Risi,<sup>1</sup> David Noone,<sup>2</sup> Christian Frankenberg,<sup>3</sup> and John Worden<sup>3</sup>

Received 5 November 2012; revised 9 April 2013; accepted 14 May 2013; published 22 July 2013.

[1] Climate models suggest an important role for land-atmosphere feedbacks on climate, but exhibit a large dispersion in the simulation of this role. We focus here on the role of continental recycling in the intraseasonal variability of continental moisture, and we explore the possibility of using water isotopic measurements to observationally constrain this role. Based on water tagging, we design a diagnostic, named D1, to estimate the role of continental recycling on the intraseasonal variability of continental moisture simulated by the general circulation model LMDZ. In coastal regions, the intraseasonal variability of continental moisture is mainly driven by the variability in oceanic moisture convergence. More inland, the role of continental recycling becomes important. The simulation of this role is sensitive to model parameters modulating evapotranspiration. Then we show that  $\delta D$  in the low-level water vapor is a good tracer for continental recycling, due to the enriched signature of transpiration. Over tropical land regions, the intraseasonal relationship between  $\delta D$  and precipitable water, named D1\_iso, is a good observational proxy for D1. We test the possibility of using D1\_iso for model evaluation using two satellite data sets: GOSAT and TES. LMDZ captures well the spatial patterns of D1\_iso, but underestimates its values. However, a more accurate description of how atmospheric processes affect the isotopic composition of water vapor is necessary before concluding with certitude that LMDZ underestimates the role of continental recycling.

**Citation:** Risi, C., D. Noone, C. Frankenberg, and J. Worden (2013), Role of continental recycling in intraseasonal variations of continental moisture as deduced from model simulations and water vapor isotopic measurements, *Water Resour. Res.*, 49, 4136–4156, doi:10.1002/wrcr.20312

## 1. Introduction

### 1.1. Goals

[2] Many studies have suggested an important role of the land surface on atmospheric conditions at a broad range of time scales [Rowntree and Bolton, 1983; Nicholson, 2000; Koster et al., 2004; Seneviratne et al., 2010; Gimeno et al., 2012]. Land-atmosphere feedbacks are particularly important for the intraseasonal variability of precipitation [Beljaars et al., 1996] and extreme events such as droughts or floods [Dirmeyer and Brubaker, 1999; Pal and Eltahir, 2001; Seneviratne et al., 2006; Zaitchik et al., 2006;

Fischer et al., 2007]. However, climate models exhibit a large dispersion in the simulation of land-atmosphere feedbacks [Koster et al., 2002, 2004; Lawrence and Slingo, 2005; Koster et al., 2006; Guo et al., 2006; Wei and Dirmeyer, 2010]. It is however difficult to discriminate which model represents land-atmosphere feedbacks in the most realistic way. The motivation underlying this paper is to find observational constraint for land-atmosphere feedbacks. These feedbacks are complex in the sense that precipitation might be either enhanced or decreased when the soil is wetter depending on conditions [Findell and Eltahir, 2003a, 2003b; Ferguson and Wood, 2011].

[3] Land-atmosphere feedbacks can be either local (sometimes called “direct”) or regional (sometimes called “indirect”).

[4] Local feedbacks involve the effect of surface fluxes on the local atmospheric conditions. Positive or negative effects of soil moisture on subsequent precipitation are possible depending on large-scale atmospheric conditions [Betts, 1992; de Ridder, 1997; Findell and Eltahir, 2003a, 2003b; Ek and Holtslag, 2004; Santanello et al., 2009, 2011; Tuinenburg et al., 2011; Ferguson and Wood, 2011; Ferguson et al., 2012], on the spatial scale of soil moisture anomalies [Taylor et al., 2011], on the type of convective system [Taylor et al., 2009] or on whether the variable of interest is precipitation intensity or frequency [d’Odorico

Additional supporting information may be found in the online version of this article.

<sup>1</sup>Laboratoire de Météorologie Dynamique, Institut Pierre Simon Laplace, CNRS, Paris, France.

<sup>2</sup>Department of Atmospheric and Oceanic Sciences, CIRES, University of Colorado, Boulder, Colorado, USA.

<sup>3</sup>Jet Propulsion Laboratory, California Institute of Technology, Pasadena, California, USA.

Corresponding author: C. Risi, LMD/IPSL, CNRS, Paris 75005, France. (camille.risi@lmd.jussieu.fr)

©2013. American Geophysical Union. All Rights Reserved.  
0043-1397/13/10.1002/wrcr.20312

and Porporato, 2004]. On the one hand, if the soil is wetter, evapo-transpiration increases, which moistens the boundary layer, lowers the condensation level and favors convection [e.g., Betts, 1992; Taylor and Lebel, 1998; Santanello et al., 2009; Lintner et al., 2012]. On the other hand, if the soil is drier, then latent heat fluxes decrease at the expense of sensible heat flux, which warms the boundary layer, leads to more vigorous thermals and higher boundary layer top, and favors convection triggering [e.g., Porporato, 2009; Santanello et al., 2009; Westra et al., 2012; Taylor et al., 2012]. In models, the relative importance of these two effects may additionally depend on the model physics and resolution [Hohenegger et al., 2009]. Local feedbacks can also involve small-scale soil moisture gradients and associated mesoscale circulations [Taylor et al., 2007, 2009, 2011] and radiative effects of clouds [Schär et al., 1999; Betts, 2004; Schlemmer et al., 2011, 2012].

[5] Regional feedbacks involve the effect of surface fluxes on remote atmospheric conditions and on large-scale circulation. Positive and negative effects are possible depending on conditions. On the one hand, if the soil is wetter, then the evapo-transpiration increases. This moistens the atmosphere and favors convection downstream air mass trajectories [Eltahir and Bras, 1994]. For example, this can contribute to lower precipitation downstream of deforested areas [Spracklen et al., 2012]. This can also contribute to the persistence of droughts [Rodríguez-Iturbe et al., 1991a, 1991b; Entekhabi et al., 1992]. On the other hand, if the soil is drier, the surface temperature increases which favors large-scale convergence of tropospheric humidity, and thus favors convection [Kleidon and Heimann, 2000; Cook et al., 2006; Goessling and Reick, 2011]. For example, this may contribute to lower precipitation over irrigated regions [Lee et al., 2009a; Saeed et al., 2009; Guimberteau et al., 2012]. Storms might also become more intense despite a less frequent triggering [Lee et al., 2012]. In the case of a positive feedback, continental recycling increases; in the case of a negative feedback, it decreases.

[6] This paper focuses on regional-scale feedbacks. Such feedbacks have been less studied than local feedbacks because it is often thought that the effect of the direct input of water vapor through continental recycling is small, due to the long residence time scale (10 days) of water vapor in the atmosphere [McDonald, 1962]. The importance of continental recycling however strongly depends on the region considered [Koster et al., 1986], on the spatial scale considered [Budyko, 1974; Burde et al., 1996; Trenberth, 1999] and on the methodology used to quantify continental recycling [Eltahir and Bras, 1996]. Progress have been made to more robustly quantify the sources and sinks of precipitation and of water vapor (review by Gimeno et al. [2012]) and underline the importance of continental recycling in some continental regions [Dominguez et al., 2006; Gimeno et al., 2010; van der Ent et al., 2010]. Quantifying the role of continental recycling on precipitation usually involves regional atmospheric water budgets based on reanalyses, on a combination of reanalyses and observations [Eltahir and Bras, 1996; Gong and Eltahir, 1996; Schär et al., 1999; Bosilovich and Schubert, 2002; Dirmeyer and Brubaker, 2007; Dominguez and Kumar, 2008; Dirmeyer et al., 2008, 2009] or on models [Brubaker et al., 1994]. There are, however, two drawbacks to this approach. First,

it is difficult for such moisture budgets to accurately take into account the effect of mixing and of subgrid scale water vapor transport, sources, and sinks. Second, reanalyses are model products and their derived budgets are difficult to evaluate observationally. In this paper, to circumvent the first drawback, we use a water tagging approach [e.g., Jous-saume et al., 1984; Koster et al., 1986; Numaguti et al., 1999; Yoshimura et al., 2004; Risi et al., 2010b], which accurately tracks the water vapor through each transport, mixing, and phase change process online in a global model. To deal with the second issue, we explore the possibility of using water isotopic measurements.

[7] The water molecule has several isotopologues. The most common isotopologue is  $\text{H}_2^{16}\text{O}$  (hereafter called  $\text{H}_2\text{O}$ ), but heavier isotopologues are also found:  $\text{HD}^{16}\text{O}$  (hereafter call HDO, with D standing for deuterium) and  $\text{H}_2^{18}\text{O}$ . The water vapor isotopic composition (e.g., the concentration in HDO) is sensitive to the evaporative origin. For example, in the tropics, water evaporated from land surface is more enriched in heavy isotopes than water evaporated from the ocean [Gat, 1996]. Several studies have tried to exploit this property to infer continental recycling or to partition it into evaporation and transpiration, using isotopic measurements in the precipitation [Salati et al., 1979; Gat and Matsui, 1991]. However, precipitation is strongly affected by postcondensational processes [Stewart, 1975; Lee and Fung, 2008; Risi et al., 2010a]. The isotopic composition of water vapor more directly reflects the moisture origin. The development of water vapor isotopic measurements from satellite now offers a unique opportunity to exploit the water isotopic composition as an indication for continental recycling [Risi et al., 2010b].

[8] The goal of our paper is thus to explore the possibility to use water isotopic measurements from satellites to observationally constrain the role of continental recycling on the intraseasonal variability of precipitation. More specifically, given the close relationship between precipitation and precipitable water ( $W$ ) in the tropics [Raymond, 2000; Bretherton et al., 2004], we will focus on evaluating the role of continental recycling on the intraseasonal variability of  $W$  in the tropics.

## 1.2. Overview of the Methodology

[9] To achieve this goal, we use an atmospheric general circulation model (GCM) coupled to a land surface model. Our strategy has three steps. First, we develop a diagnostic for the role of continental recycling variability on the intraseasonal variability of  $W$ . This diagnostic is called D1 and is calculated from a GCM simulation in which water vapor from different origins is tagged. We quantify and discuss the role of continental recycling in this simulation. Two sensitivity tests to the land surface physics are also presented in which the role of continental recycling is either larger or weaker than in the control, as quantified by D1.

[10] Second, we try to find an observation-based proxy for D1 to identify the simulation which has the most realistic role of continental recycling. While D1 is not directly observable, our hypothesis is that water vapor isotopic composition measurements may track continental recycling and its intraseasonal variations. In addition to water tagging, our GCM is also equipped with water isotopic diagnostics. We focus on the HDO/ $\text{H}_2\text{O}$  ratio of water vapor,

expressed in ‰ as anomalies relatively to the ocean surface:  $\delta D = \left( \frac{\text{HDO}/\text{H}_2\text{O}}{(\text{HDO}/\text{H}_2\text{O})_{\text{SMOW}}} - 1 \right) \cdot 1000$ , where SMOW is the standard mean ocean water [Dansgaard, 1964]. We show a good relationship between continental recycling and lower tropospheric  $\delta D$  at the intraseasonal time scales over several regions. Based on those results, and on the availability of isotopic observations, we propose an isotope-based, observable proxy for D1, named D1\_iso.

[11] Third, we compare simulated D1\_iso with data, to assess to what extent data can help identify the most realistic simulation in terms of D1. To do so, we use two satellite data sets which are sensitive to the isotopic composition of the boundary layer water vapor and which have a good spatio-temporal coverage: the GOSAT (Greenhouse gases Observing SATellite) satellite data set [Frankenberg *et al.*, 2012] and the new version of the TES (Tropospheric Emission Spectrometer) retrievals [Worden *et al.*, 2012a].

[12] The paper is organized according to these three steps. After a description of the model simulations, of the data sets and of the methodology (section 2), we quantify the role of continental recycling on intraseasonal variability of  $W$  in our simulations (section 3). We show the link between continental recycling and water vapor isotopic composition in section 4, and discuss a possible isotopic-based observable constraint to our model simulations in section 5. We conclude in section 6.

## 2. Material and Methods

### 2.1. Models

[13] We use the LMDZ4 (Laboratoire de Météorologie Dynamique-Zoom version 4) model, which is the atmospheric component of the IPSL-CM4 and IPSL-CM5A ocean-atmosphere coupled models [Marti *et al.*, 2005; Dufresne *et al.*, 2012] used in CMIP3 and CMIP5 [Meehl *et al.*, 2007]. It is used with a resolution of  $2.5^\circ$  in latitude,  $3.75^\circ$  in longitude and 19 vertical levels. The physical package is comprehensively described in Hourdin *et al.* [2006]. The isotopic version of LMDZ, named LMDZ-iso, is described in detail in Risi *et al.* [2010c]. Isotopic processes are represented in a way similar to other isotopic GCMs [Jouzel *et al.*, 1987, 1991; Hoffmann *et al.*, 1998; Noone and Simmonds, 2002; Schmidt *et al.*, 2005; Lee *et al.*, 2007a; Yoshimura *et al.*, 2008; Tindall *et al.*, 2009]. Isotopic processes associated with rain reevaporation, crucial in controlling the precipitation composition [Lee and Fung, 2008; Bony *et al.*, 2008; Risi *et al.*, 2010c] and vapor composition [Worden *et al.*, 2007; Field *et al.*, 2010] are represented in detail [Bony *et al.*, 2008].

[14] The default land surface scheme in LMDZ is a simple bucket in which no distinction is made between bare soil evaporation and transpiration, and no fractionation is considered during evapo-transpiration [Risi *et al.*, 2010c]. Since we focus here on land-atmosphere interaction, a more accurate description of isotopic fractionation during land surface evapo-transpiration is necessary. Therefore, LMDZ-iso was coupled with the ORCHIDEE-iso land surface model [Ducoudré *et al.*, 1993; Krinner *et al.*, 2005]. This model includes a two-layer soil model [Choisnel *et al.*, 1995]. The very low vertical resolution of the soil in this model may impact the realism of the simulation [de Rosnay *et al.*, 2000]. The model decomposes evapotranspiration

through evaporation of canopy-intercepted water, bare soil evaporation, plant transpiration, and snow sublimation. For simplicity and for easier interpretation of the results, we disabled the dynamic vegetation model [Sitch, 2003], the carbon allocation model [Krinner *et al.*, 2005] and the canopy interception module. Vegetation fractions are prescribed.

[15] The isotopic implementation in ORCHIDEE is described in detail in [Risi, 2009]. Water stable isotopes are passively transported between the different water reservoirs by nonfractionating water fluxes. The isotopic composition of soil water is assumed homogeneous vertically and equal to the weighted average of the two soil layers. We assume that surface runoff has the composition of the excess inflow into the soil, that is, precipitation or snow melt, and that drainage has the composition of soil water [Gat, 1996]. Isotope fractionation during evaporation of bare soil is modeled using Craig and Gordon [1965] equation and the kinetic fractionation formulated by Mathieu and Bariac [1996]. Isotope fractionation processes during transpiration [Washburn and Smith, 1934; Barnes and Allison, 1988] and snow sublimation [Hoffmann *et al.*, 1998; Noone and Simmonds, 2002] are neglected. ORCHIDEE-iso has been evaluated against measurements of soil, stem, leaf, river, and precipitation water both in stand-alone mode at several instrumented sites and in LMDZ-coupled mode [Risi, 2009]. The coupled LMDZ-ORCHIDEE model was also evaluated and used in Risi *et al.* [2010b].

### 2.2. Simulation Setup

[16] LMDZ is forced by observed sea surface temperatures following the AMIP protocol [Gates, 1992]. To ensure a realistic large-scale circulation and daily variability [Yoshimura *et al.*, 2008; Risi *et al.*, 2010c], horizontal winds at each vertical level are nudged by ECMWF (European Centre for Medium-Range Weather Forecasts) reanalyses [Uppala *et al.*, 2005].

[17] Water tagging is available in both LMDZ and ORCHIDEE [Risi *et al.*, 2010b]. To track the origin of water vapor and continental recycling, nine tracers were used:  $\text{H}_2\text{O}$  tracer emitted from bare soil or snow evaporation,  $\text{H}_2\text{O}$  tracer emitted from plant transpiration,  $\text{H}_2\text{O}$  tracer emitted from the ocean, and  $\text{H}_2^{18}\text{O}$  and HDO emitted from these three sources.

[18] In addition, we perform two sensitivity tests (Table 1) in which the role of continental recycling on  $W$  variations is different from that in the control simulation. This allows us to assess whether two simulations, in which the role of continental recycling on  $W$  variations is different, can be discriminated based on their water isotopic composition. First, in the “baresoil” simulation, we modify the calculation of the bare soil fraction as a function of the leaf area index (LAI). In the control simulation, the bare soil fraction decreases linearly with LAI [Ducoudré *et al.*, 1993], whereas in the “baresoil” simulation, it decreases exponentially with LAI [d’Orgeval, 2006]. As a result, in “baresoil” the bare soil fraction is lower over most regions. Second, in the “rveg” simulation, we reduce the stomatal resistance. In the control simulation, the stomatal resistance is calculated as a function of radiative fluxes and LAI. In the “rveg” simulation, we keep the same calculation but divide the result by a factor of 5.

[19] For computer limitation reasons, simulations were run for 3 years and the last year was analyzed. Simulations



**Table 1.** Time Period and Characteristics of the LMDZ and LMDZ-ORCHIDEE Simulations Used in This Paper

Name	Year	Coupling With ORCHIDEE	Bare Soil Function	Stomatal Resistance	Water Tagging
Control	2006	Yes	<i>Ducoudré et al.</i> [1993]	0.5	Yes
Baresoil	2006	Yes	<i>d'Orgeval</i> [2006]	0.5	Yes
rveg	2006	Yes	<i>Ducoudré et al.</i> [1993]	0.1	Yes
LMDZ	1997–2012	No	None	None	No

are performed with perpetual 2006 conditions, 2006 being chosen arbitrarily. Simulations are started from a control perpetual-2006 simulation that had the time to equilibrate during 20 years. Despite the shortness of the simulations, the nudging ensures that the difference between the sensitivity tests is due to differences in the physical content of the model rather than to internal variability.

### 2.3. GOSAT Data

[20] Similar to SCIAMACHY [*Frankenberg et al.*, 2009], GOSAT measurements enable to retrieve the total-column water vapor content in both H<sub>2</sub>O (i.e., precipitable water  $W$ ) and HDO [*Frankenberg et al.*, 2012]. From these retrievals, column-integrated  $\delta D$  is calculated. Since most of the total-column vapor is in the lower troposphere, column-integrated  $\delta D$  is strongly weighted toward the  $\delta D$  of the boundary layer [*Frankenberg et al.*, 2009]. We use measurements from April 2009 to June 2011. The precision of each measurement is 20–40‰, but it can be refined by averaging several measurements. For a first brief study of GOSAT  $\delta D$  data uncertainty, please refer to *Boesch et al.* [2012]. Observed column-integrated H<sub>2</sub>O and HDO have been corrected following *Frankenberg et al.* [2012]. No absolute calibration exists for column-integrated  $\delta D$  and we thus focus on spatiotemporal variations only.

[21] We select only GOSAT measurements that met several quality criteria. Cloud scenes are screened out. Retrieved  $W$  must agree within 30% with ECMWF reanalyses. Errors on retrieved  $W$  and column-integrated HDO must be lower than 15%. Retrieval  $\chi^2$  [*Frankenberg et al.*, 2012] must be lower than 0.3. Retrieved  $\delta D$  must be within –900‰ and 1000‰ to exclude a few obviously anomalous values.

[22] To compare rigorously LMDZ with GOSAT, we take into account spatiotemporal sampling. This is possible only if LMDZ is nudged toward reanalysis for the GOSAT observation period. Therefore, we use an additional nudged LMDZ simulation covering 1997–2012 (Table 1). Contrary to SCIAMACHY but similar to TES [*Worden et al.*, 2006], the retrieval method for GOSAT yields averaging kernels that describe the sensitivity of the retrieved  $W$  and column-integrated  $\delta D$  to the different atmospheric levels. For a rigorous model-data comparison, we apply averaging kernels to the model outputs [*Risi et al.*, 2012a].

[23] When interpreting HDO/H<sub>2</sub>O remote sensing data, several limitations must be taken into account. First, HDO/H<sub>2</sub>O retrievals depend on spectroscopic parameters that are typically determined by laboratory measurements. These measurements are difficult especially for the relatively weak lines in the near infrared [*Scheepmaker et al.*, 2012]. Spectroscopic biases could further depend on humidity content. Second, the sensitivity of the measurements

needs to be considered, and a priori constraints can significantly affect the retrievals [*Boesch et al.*, 2012]. The HDO sensitivity depends on the H<sub>2</sub>O content of the atmosphere. To quantify this effect, we calculated the difference between convolved total-column  $\delta D$  and raw total-column  $\delta D$  in the LMDZ model, and analyzed the link with precipitable water. We find that in some regions, when the atmosphere is drier, the sensitivity of the instrument is such that retrieved  $\delta D$  is artificially reduced compared to real  $\delta D$  (supporting information). As a consequence, relationships between  $\delta D$  and  $W$  may be distorted (supporting information). When convolving LMDZ outputs with averaging kernels, this effect is taken into account so that convolved outputs, and GOSAT retrievals are comparable.

### 2.4. TES Data

[24] TES measurements enable to retrieve some information on the vertical distribution of specific humidity ( $q$ ) and  $\delta D$  in the troposphere. While a first processing of the data had led to  $\delta D$  retrievals being mainly sensitive around 600 hPa [*Worden et al.*, 2006], a new processing leads to enhanced vertical sensitivity from 900 to 400 hPa [*Worden et al.*, 2012a]. We use measurements from 2004 to 2008 compiled into the so-called “lite product” available on <http://tes.jpl.nasa.gov/data/>. The precision of each measurement is about 30‰ at low levels, but as for GOSAT, it can be refined by averaging several measurements. We select only TES measurements with a valid quality flag and a degree of freedom of the signal (DOFS) greater than 0.5. On average over the tropics, the DOFS of the retrievals that we use is 1.8. Therefore, TES has a larger DOFS than GOSAT, whose DOFS is one since it retrieves column abundances.

[25] A correction was applied on observed  $\delta D$  following the calibration study of *Worden et al.* [2010]. However, since absolute calibration remains uncertain, as for GOSAT we will focus on spatio-temporal variations only.

[26] To compare directly the TES data with the GOSAT data, we calculate  $W$  and column-integrated  $\delta D$  from the TES profiles. Column-integrated  $\delta D$  is consistent (spatial correlation greater than 0.5) with  $\delta D$  retrieved at any single level between about 900 and 700 hPa.

[27] As for GOSAT, to compare LMDZ to TES, we take into account spatio-temporal sampling and instrument sensitivity through collocation and convolution with TES averaging kernels [*Risi et al.*, 2012a] using the nudged 1997–2012 LMDZ simulation. Model-prior differences in humidity in the upper troposphere may distort convolved  $\delta D$  profiles, as was the case for CH<sub>4</sub> in *Worden et al.* [2012b], but this effect is masked when considering total-column  $\delta D$ .

[28] As for GOSAT, limitations of the remote sensing data should be taken into account [*Worden et al.*, 2006;

Schneider and Hase, 2011]. Spectroscopic biases are possible. The bias in  $\delta D$  depends on the sensitivity of the measurement [Worden *et al.*, 2010], which may depend on the  $H_2O$  and  $HDO/H_2O$  content. Direct dependence of the  $\delta D$  bias on atmospheric conditions were not considered [Worden *et al.*, 2010], but they might exist. In addition, the sensitivity of the measurement, including limited vertical resolution and effect of a priori constraint, needs to be considered. The HDO sensitivity depends, among many other factors, on the  $H_2O$  content of the atmosphere. As a consequence, relationships between  $\delta D$  and  $W$  may be distorted. The effect of instrument sensitivity is to slightly enrich or deplete column-integrated  $\delta D$  on days when the atmosphere is drier, depending on regions (supporting information).

### 2.5. Water Tagging Approach to Quantify the Role of Continental Recycling on Intraseasonal Moisture Variability

[29] As introduced in section 1.2, we use the water tagging approach to quantify the role of continental recycling in intraseasonal variations of precipitable water. By intraseasonal, we mean the daily variability within a given season. Therefore, hereafter, we use daily outputs and data and we focus on the June-July-August (JJA) and December-January-February (DJF) seasons. This limits contamination by seasonal variations that occur mainly during the transition seasons.

[30] First, we quantify the continental recycling by the fraction of the vapor originating from continental evaporation in the lowest-level vapor, noted  $r_{con}$ . We define continental evaporation as the sum of the bare-soil evaporation, snow sublimation, and transpiration. We choose to estimate  $r_{con}$  from the lowest-level vapor of the model because (1) this vapor is the most representative of the moisture convergence and (2) this vapor is the most directly affected by continental evaporation. In the tropics, the fraction of the vapor originating from continental evaporation increases with altitude and reaches a maximum in the upper troposphere, which is due to fast injection of continental-evaporated water vapor by deep convection over land regions. This water vapor accumulates in the tropical upper troposphere and subsides slowly in the Hadley-Walker cell. We are not interested in this effect, hence our choice to quantify  $r_{con}$  in the lowest-level vapor.

[31] The role of continental recycling in intraseasonal variations of precipitable water ( $W$ ) can be either positive or negative. If the role of continental recycling is positive, then an increase in  $W$  is associated with an increase in  $r_{con}$ . In contrast, if the increase in  $W$  is associated with an increase in moisture convergence, then this moisture convergence will bring moisture from further away and with a larger proportion of oceanic moisture. In this case, the increase in  $W$  is associated with a decrease in  $r_{con}$ . More quantitatively, we decompose the moisture  $W$  into oceanic moisture ( $W_{oce} = (1 - r_{con}) \cdot W$ ) and continental moisture ( $W_{con} = r_{con} \cdot W$ ). Therefore,  $W$  variations ( $dW$ ) can be decomposed into:

$$dW = dW_{oce} + dW_{con} = dW_{oce} + dr_{con} \cdot W + dW \cdot r_{con} \quad (1)$$

rearranging this equations yields:

$$d \ln(W) = d \ln(W_{oce}) + d \ln\left(\frac{1}{1 - r_{con}}\right) \quad (2)$$

[32] Atmospheric moisture variations can thus be decomposed into two terms: variations in oceanic moisture advection and variations in continental recycling (respectively first and second term on the right-hand side). When  $d \ln\left(\frac{1}{1 - r_{con}}\right)$  is positively correlated with  $d \ln(W)$ , then continental recycling contributes positively to  $W$  variations. In this case, continental recycling contributes all the more as  $\frac{d \ln\left(\frac{1}{1 - r_{con}}\right)}{d \ln(W)}$  is large. For example, when  $\frac{d \ln\left(\frac{1}{1 - r_{con}}\right)}{d \ln(W)} = 1$ , then  $r_{con}$  variations are responsible for 100% of  $W$  variations. In contrast, when  $d \ln\left(\frac{1}{1 - r_{con}}\right)$  is negatively correlated with  $d \ln(W)$ , then continental recycling contributes negatively to  $W$  variations. In this case, oceanic moisture convergence contributes positively. The role of moisture convergence is all the larger as  $\frac{d \ln\left(\frac{1}{1 - r_{con}}\right)}{d \ln(W)}$  is largely negative. Hereafter, we quantify the role of continental recycling on moisture variations by the diagnostic D1:

$$D1 = \frac{d \ln\left(\frac{1}{1 - r_{con}}\right)}{d \ln(W)} \cdot 100 \quad (3)$$

expressed in percentage.

## 3. Simulated Role of Continental Recycling on Intraseasonal Moisture Variability

### 3.1. Simulated Continental Recycling

[33] Figure 1 shows that  $r_{con}$  values range from <5% over most of the oceans up to 85% in Siberia in summer. These values are very consistent with previous estimates using water tagging [Koster *et al.*, 1986; Yoshimura *et al.*, 2004] or moisture budgets at the global scale [van der Ent *et al.*, 2010; Goessling and Reick, 2011], both in magnitude and in spatial and seasonal patterns. They are however much larger than estimates of recycling rates based on regional water budgets [Budyko, 1974; Brubaker *et al.*, 1993; Trenberth, 1999; Schär *et al.*, 1999]. Those recycling rates estimates are not directly comparable to  $r_{con}$  because they represent the fraction of the precipitation or of the vapor originating from evapo-transpiration within a domain of interest, and results depend on the size [Trenberth, 1999] and shape of the domain [van der Ent and Savenije, 2011].

### 3.2. Role of Continental Recycling on Intraseasonal Moisture Variability for the Control Simulation

[34] Figures 2a–2d show the daily correlation and slope (D1) of  $\ln\left(\frac{1}{1 - r_{con}}\right)$  as a function of  $\ln(W)$  for JJA and DJF. In coastal regions where the influence of moisture advection from the ocean is strong, the correlation and D1 are negative (coastal United States, Europe, coastal northeastern South America, India during the monsoon season, coastal western Africa during the monsoon season). In high latitudes where most of the vapor originates from continental recycling, D1 reaches the highest positive values. In South America, during both seasons, there is a gradient toward the interior following air mass trajectories: intraseasonal variations of  $W$  are driven mainly by large-scale convergence of oceanic moisture near the coast, but

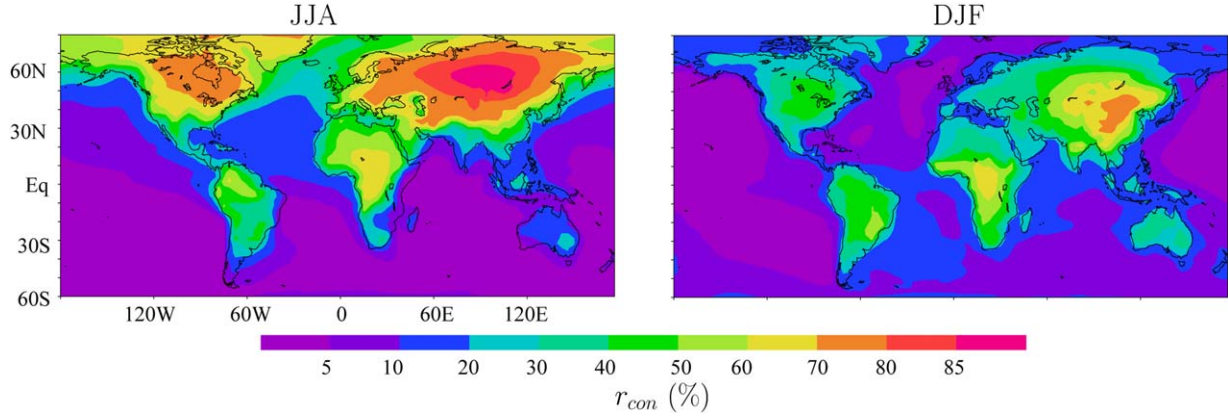


**Figure 1.** Proportion of the low-level vapor originating from continental recycling ( $r_{con}$ ) in (a) JJA and (b) DJF as diagnosed from water tagging.

become more and more driven by changes in continental recycling toward the interior. The same effect can be seen in the Sahel during summer.

[35] Quantitatively, in South America for example, D1 goes from about  $-100\%$  near the coast to about  $100\%$  in the Amazon interior. This means that near the coast, when  $W$  doubles, it is associated with a tripling of the oceanic contribution and it is attenuated by a reduction of  $r_{con}$  (i.e., according to equation (2),  $d\ln(W) = +100\%$ ,  $d\ln(W_{oce}) =$

$+200\%$  and  $d\ln\left(\frac{1}{1-r_{con}}\right) = -100\%$ ). In the Amazon interior, when  $W$  doubles, it is fully explained by the increase in  $r_{con}$  (i.e.,  $d\ln(W) = +100\%$ ,  $d\ln(W_{oce}) = 0\%$  and  $d\ln\left(\frac{1}{1-r_{con}}\right) = +100\%$ ).

[36] Our maps of the role of continental recycling on  $W$  variability are not directly comparable to the maps of the magnitude of land-atmosphere feedbacks by *Koster et al.* [2004], who quantified the sum of all local and regional

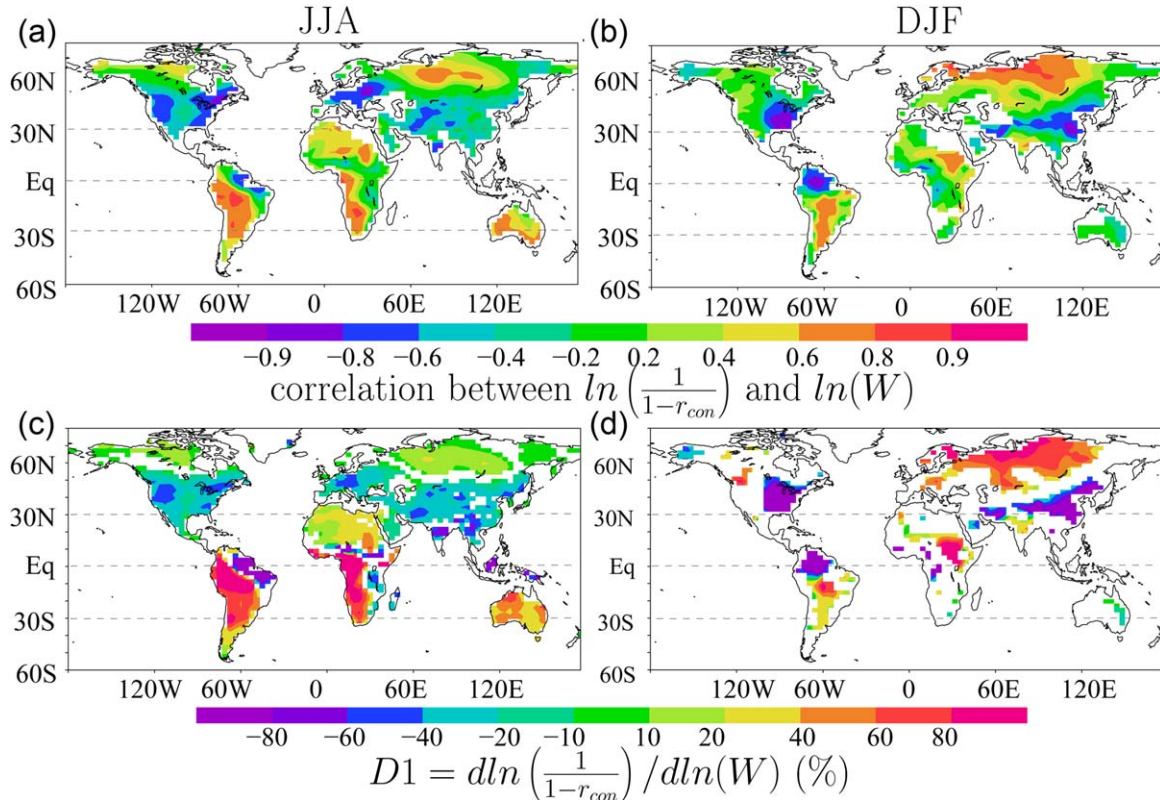


**Figure 2.** (a) Daily correlation coefficient ( $r$ ) of the linear regression between  $\ln(W)$  and  $\ln\left(\frac{1}{1-r_{con}}\right)$  in JJA. (c) Slope of this linear regression, where the correlation coefficient is greater than 0.2 (Figures 2b and 2d). Same as Figures 2a and 2c but in DJF.



effects of land moisture, while we quantify just the regional effect through continental recycling. For example, the thermodynamical role of surface fluxes on atmospheric instability and on the boundary layer activity [e.g., *Findell and Eltahir*, 2003a] is implicitly included in *Koster et al.* [2006] but not in our study.

[37] Still we can compare our maps with some previous studies. Most previous studies have focused on linking moisture origin to precipitation variability rather than to  $W$  as we do here. Therefore, their results and ours are not directly comparable, though precipitation and  $W$  are significantly correlated over most of the globe. Most of these studies have so far focused on Europe and on the United States. In Europe, our negative sign is consistent with *Schär et al.* [1999], who found that the moisture convergence effect dominates over the continental recycling effect for summer precipitation. It is also consistent with *Dufour and Ducrocq* [2011], who found an oceanic origin for extreme precipitation events and floods in southern France. In the central plains of the United States, our negative sign is consistent with *Zangvil et al.* [2004] and *Dominguez and Kumar* [2008], who found anticorrelation between precipitation and recycling rates at intraseasonal time scales. *Dominguez et al.* [2008] however found a positive correlation of continental recycling with summer precipitation variability in southwestern United States at the interannual scale, while we find a negative correlation there at the intraseasonal scale.

### 3.3. Sensitivity to Land Surface Model Representation

[38] The goal of our sensitivity tests is to compare simulations in which the role for continental recycling on intraseasonal variations of  $W$  is different. We check that this difference is reflected by our D1 diagnostic (Figure 3).

[39] When the bare soil fraction is reduced, D1 decreases over most of the tropics: South America, Southeast Asia, and Australia in both seasons, in western Africa in winter and in southwestern United States in winter (Figures 3a and 3b). Some regions behave differently due to different atmospheric contexts, but here we focus on the broad patterns. On average over the tropics, D1 values are about half in “baresoil” compared to that in the control.

[40] In contrast, when the stomatal resistance is reduced, D1 increases over most of the tropics: South America and the Congo basin in both seasons, southern Africa in summer (Figures 3c and 3d). On average over the tropics, D1 values are about 50% larger in “rveg” compared to the control.

[41] The decrease of D1 as the bare soil fraction decreases can be explained as follows: bare soil areas are more sensitive than vegetated areas to changes in the soil water content. Over bare soil, a small change in soil water content will lead to stronger changes in evaporation, thus leading to stronger changes in continental recycling. Over vegetated areas, plants can transpire water with a similar rate over a broader range of soil water content. Therefore, as the bare-soil fraction decreases, the  $r_{con}$  variations at intraseasonal variations are smaller. This interpretation is confirmed by the fact that on average over the tropics, the correlation between soil water content and evapo-transpiration ratio to potential evapotranspiration [Milly, 1992] is lower in “baresoil” than in the control simulation (Figure 3e). In contrast, the increase

of D1 as the stomatal resistance decreases can be explained as follows: reduced stomatal resistance leads to stronger transpiration, which dehydrates the soil. At lower soil water contents, evapo-transpiration becomes more sensitive to soil water content. This interpretation is also confirmed by the fact that on average over the tropics, the correlation between soil water content and evapo-transpiration ratio to potential evapotranspiration is higher in “rveg” than in the control simulation (Figure 3e). The important role of the coupling between soil water and evapo-transpiration in determining the intensity of land-atmosphere feedbacks was already pointed out by *Guo et al.* [2006].

[42] In the following, we will explore whether isotopic observations can help us assess which simulation has the most realistic role of continental recycling in intraseasonal variation of  $W$ .

## 4. Isotopic Signature of Continental Recycling and of its Variability

### 4.1. Isotopic Signature of Evaporative Sources

[43] First, water tagging allows us to document the different isotopic signatures of each evaporative source. For comprehensiveness, we will document both the isotopic composition in terms of enrichment in heavy isotopes (quantified by  $\delta D$  or  $\delta^{18}O$ ) and in terms of the relative enrichment in HDO compared to that in  $H_2^{18}O$  (quantified by d-excess =  $\delta D - 8 \cdot \delta^{18}O$ , *Dansgaard* [1964]). We show that in the tropical low-level vapor, each evaporative origin has a distinct isotopic signature (Figure 4).

[44] Water vapor from vegetation transpiration is much more enriched than oceanic evaporation. This property may contribute to the maximum enrichment that is observed by satellites over tropical land masses [Worden et al., 2007; Brown et al., 2008; Frankenberg et al., 2009]. This is because lighter isotopes evaporate more easily from free liquid surfaces. With typical tropical oceanic conditions (25°C surface temperature, 75% humidity,  $\delta^{18}O \simeq -12\text{‰}$ , and  $\delta D \simeq -83\text{‰}$  in ambient vapor), ocean evaporation is  $\simeq 5\text{‰} \simeq 5\text{‰}$  more enriched in  $H_2^{18}O$  and  $\simeq 5\text{‰} \simeq 5\text{‰}$  more enriched in HDO than the ambient vapor. In contrast, transpiration is not associated with fractionation relatively to soil water, because there is no fractionation during root extraction [Washburn and Smith, 1934; Barnes and Allison, 1988; Flanagan and Ehleringer, 1991] and all water extracted by the root needs to be transpired shortly after. Soil water originates from precipitation, which is to first order at equilibrium with the ambient vapor [Field et al., 2010]. For typical tropical conditions (25°C), precipitation is  $\simeq 10\text{‰} \simeq 10\text{‰}$  more enriched in  $H_2^{18}O$  and  $\simeq 80\text{‰} \simeq 80\text{‰}$  more enriched in HDO than the ambient vapor. Note that this reasoning holds in the tropics only. In the extra-tropics, under depleted water vapor the oceanic evaporation becomes more enriched than the transpiration of precipitation (e.g., for typical North Atlantic conditions, with 5°C surface temperature, 75% humidity,  $\delta^{18}O \simeq -17\text{‰}$ , and  $\delta D \simeq -130\text{‰}$  in ambient vapor, ocean evaporation is  $\simeq 18\text{‰} \simeq 18\text{‰}$  and  $\simeq 130\text{‰} \simeq 130\text{‰}$  more enriched in  $H_2^{18}O$  and HDO than the ambient vapor, while transpiration of precipitation at equilibrium with the ambient vapor at 5°C is  $\simeq 11\text{‰} \simeq 11\text{‰}$  and  $\simeq 100\text{‰} \simeq 100\text{‰}$  more enriched in



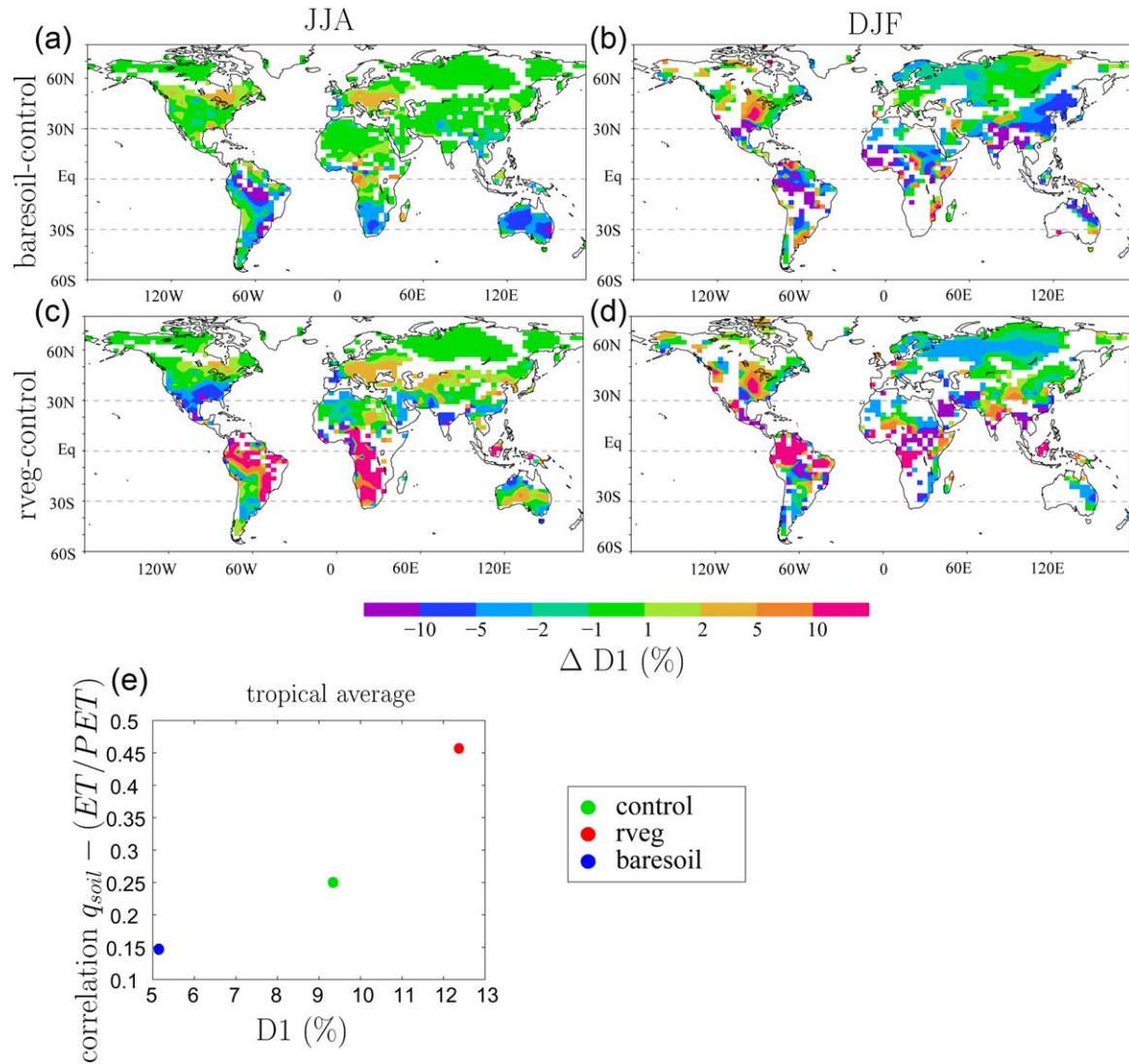


**Figure 3.** Difference in the D1 diagnostic between sensitivity tests and control simulation. The sensitivity tests are (a, b) “baresoil” (less bare soil fraction) and (c, d) “rveg” (reduced stomatal resistance) described in the section 2.2. Linear regression is calculated on daily time series for JJA (Figures 3a and 3c) and DJF and results are shown only when the correlation coefficient is greater than 0.2. These figures are the same as Figures 2b and 2d but for differences between simulations. (d) Mean correlation coefficient between soil water content and the ratio of evapo-transpiration to potential evapo-transpiration, as a function of mean slope of the linear regression between  $\ln(W)$  and  $r_{con}$ . Means are calculated over the tropics ( $30^{\circ}\text{S}$ – $30^{\circ}\text{N}$ ) and over JJA and DJF, at all locations and seasons where the correlation coefficient is greater than 0.2 for all three simulations, to represent average over the same spatial domain for all three simulations.

$\text{H}_2^{18}\text{O}$  and  $\text{HDO}$  than the ambient vapor). What remains always true, however, is that transpiration acts to enrich the overlying water vapor.

[45] Evaporation from bare soil is characterized by a stronger d-excess. This is because kinetic fractionation during the evaporation of soil water is very strong [Mathieu and Bariac, 1996; Braud *et al.*, 2009a, 2009b]. As kinetic fractionation increases, the diffusivity coefficients become important and the evaporation of  $\text{HDO}$  is favored by its high diffusivity. This property was the basis of studies trying to partition continental recycling into its transpiration and evaporation components [Gat and Matsui, 1991].

[46] These two properties could in theory be exploited to quantify both the continental recycling (with  $\delta^{18}\text{O}$  or  $\delta\text{D}$ ) and its components (with d-excess). In practice, there are observational limitations. D-excess is difficult to measure by satellite. Water vapor in situ measurements with sufficient precision are developing [e.g., Noone *et al.*, 2012; Tremoy *et al.*, 2012] but are still very scarce. Satellites can measure  $\delta\text{D}$  from space with reasonable precision and spatio-temporal coverage, but lack absolute calibration. Placing satellite measurements on Figure 4 in an attempt to quantify continental recycling is thus not applicable. This is why in this paper, we focus on

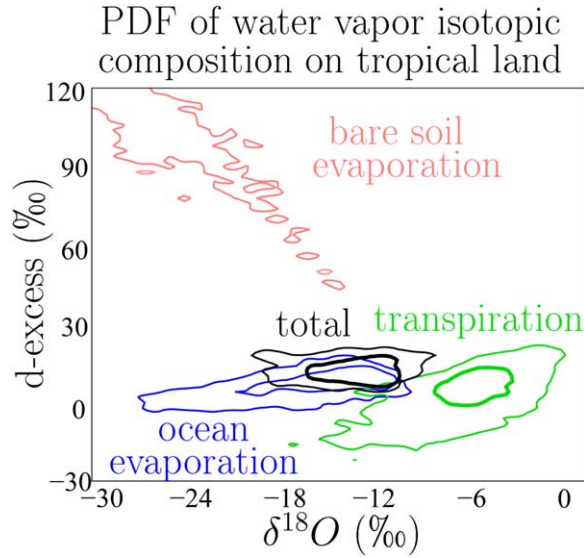


**Figure 4.** Probability density function of the isotopic composition ( $\delta^{18}\text{O}$  and d-excess) of water vapor at the lowest model level for all tropical land locations and for all days in 2006, for total vapor (black) and vapor originating from ocean evaporation (blue), land surface transpiration (green), and bare soil evaporation (pink).

exploiting the column-integrated  $\delta\text{D}$  variability at the intraseasonal scale.

#### 4.2. Intraseasonal Link

[47] To assess to what extent water isotopic measurements can be useful to estimate the role of continental recycling in intraseasonal variations of moisture, we calculate the daily correlation between  $r_{\text{con}}$  and column-integrated  $\delta\text{D}$  (Figures 5a and 5b). Since evapo-transpiration is dominated by isotopically enriched transpiration, we expect positive correlations. We can see strong positive correlations in regions of strong  $r_{\text{con}}$  (Siberia, northern America) and in tropical regions where the role of continental recycling at intraseasonal scale is strong (South America, Sahel, Congo basin, southern Africa in DJF). Overall, we find similar patterns as for D1 (2):  $\delta\text{D}$  is most sensitive to  $r_{\text{con}}$  where  $r_{\text{con}}$  has the most positive role in intraseasonal variability of moisture.

[48] Correlations would be even better if we had used  $\delta\text{D}$  in the lowest level rather than column-integrated values. Over almost all regions of the globe, the correlation between vapor  $\delta\text{D}$  at a given layer and  $r_{\text{con}}$  decreases with height (Figures 5c–5e). This is why we need  $\delta\text{D}$  measurements at the surface, in the lower troposphere or in the total column, if we want to extract information about  $r_{\text{con}}$  from such measurements.

[49] A good correlation does not necessarily imply a causal relationship, that is, that  $r_{\text{con}}$  is the main factor controlling  $\delta\text{D}$ . First, the good correlation may just be an artifact due to  $\delta\text{D}$  being controlled by other factors that correlate with  $r_{\text{con}}$  by chance. To discard this possibility, we checked that correlations between  $\delta\text{D}$  and  $r_{\text{con}}$  over land are overall preserved even if we calculate partial correlations from multiple-linear regressions of  $\delta\text{D}$  as a function of  $r_{\text{con}}$ , tem-

perature, and precipitation (not shown). Second, there could be a good correlation even though the contribution of  $r_{\text{con}}$  variations to  $\delta\text{D}$  variations are quantitatively small. To quantify the contribution of  $r_{\text{con}}$  variations to  $\delta\text{D}$  variations, we use a water-tagging-based decomposition of  $\delta\text{D}$  variations following [Risi et al., 2010b]. This decomposition is based on the fact that  $\delta\text{D} = r_{\text{con}} \cdot \delta\text{D}_{\text{con}} + (1 - r_{\text{con}}) \cdot \delta\text{D}_{\text{oce}}$ , where  $\delta\text{D}_{\text{con}}$  and  $\delta\text{D}_{\text{oce}}$  are the compositions of the vapor originating from continental recycling and oceanic evaporation, respectively. Therefore, to first order,

$$d\delta\text{D} \simeq dr_{\text{con}} \cdot (\overline{\delta\text{D}_{\text{con}} - \delta\text{D}_{\text{oce}}}) + (1 - \overline{r_{\text{con}}}) \cdot d\delta\text{D}_{\text{oce}} + \overline{r_{\text{con}}} \cdot d\delta\text{D}_{\text{con}} \quad (4)$$

[50] The overbar denotes temporal average. The first term on the right-hand side represents the impact of  $r_{\text{con}}$  variations, that is, the impact of changing origins of moisture. The second and third terms on the right-hand side quantify the impact of surface conditions during oceanic evaporation (impacting  $\delta\text{D}_{\text{oce}}$ ), the impact of surface conditions during land surface evapo-transpiration (impacting  $\delta\text{D}_{\text{con}}$ ) and the impact of all atmospheric processes along air-mass trajectories (impacting both  $\delta\text{D}_{\text{oce}}$  and  $\delta\text{D}_{\text{con}}$ ).

[51] The contribution of  $r_{\text{con}}$  variations to  $\delta\text{D}$  variations can thus be quantified in % as  $\frac{dr_{\text{con}}}{d\delta\text{D}} \cdot (\overline{\delta\text{D}_{\text{con}} - \delta\text{D}_{\text{oce}}}) \cdot 100$ , where  $\frac{dr_{\text{con}}}{d\delta\text{D}}$  is the slope of  $r_{\text{con}}$  as a function of  $\delta\text{D}$ . When this quantity is 100%, variations in  $r_{\text{con}}$  totally account for  $\delta\text{D}$  variations. When it is near 0%, other processes (i.e., second and third terms on the right-hand side of equation (4)) contribute to  $\delta\text{D}$  variations. When it exceeds 100%, other processes counterbalance the effect of  $r_{\text{con}}$ . In most regions where correlation between  $r_{\text{con}}$  and  $\delta\text{D}$  is greater than 0.4,  $r_{\text{con}}$  variations contribute for more than 40% of  $\delta\text{D}$  variations (Figure 6). On average, over all tropical regions where the correlation between  $r_{\text{con}}$  and  $\delta\text{D}$  is greater than 0.4,  $r_{\text{con}}$  variations contribute for 87% of  $\delta\text{D}$  variations. In particular, in western Africa in both seasons, in the Congo basin in DJF and in South America in JJA,  $\delta\text{D}$  variations are mainly caused by  $r_{\text{con}}$  variations. In the Sahel in JJA, this is consistent with Risi et al. [2010b]. In the Amazon in DJF,  $r_{\text{con}}$  contributes a bit less to  $\delta\text{D}$  variations. The  $\delta\text{D}$  variations in this region and season might be partly associated with convective activity [e.g., Vimeux et al., 2005, 2011]. Similarly in high latitudes (e.g., Siberia),  $r_{\text{con}}$  variations contribute less to  $\delta\text{D}$  variations. The  $\delta\text{D}$  variations in these regions are also probably controlled by temperature [e.g., Kurita et al., 2004].

#### 4.3. Isotopic Proxy for the Water-Tagging-Based Diagnostic

[52] Based on these encouraging results, we propose an observable proxy for D1, named D1\_iso, calculated as the slope of column-integrated  $\delta\text{D}$  as a function of  $\ln(W)$ :

$$\text{D1\_iso} = \frac{d\delta\text{D}}{d\ln(W)}$$

[53] We use  $\ln(W)$  because the relationship of  $\delta\text{D}$  as a function of  $W$  is nonlinear [e.g., Frankenberg et al., 2009; Galewsky and Hurley, 2010] and because the Rayleigh

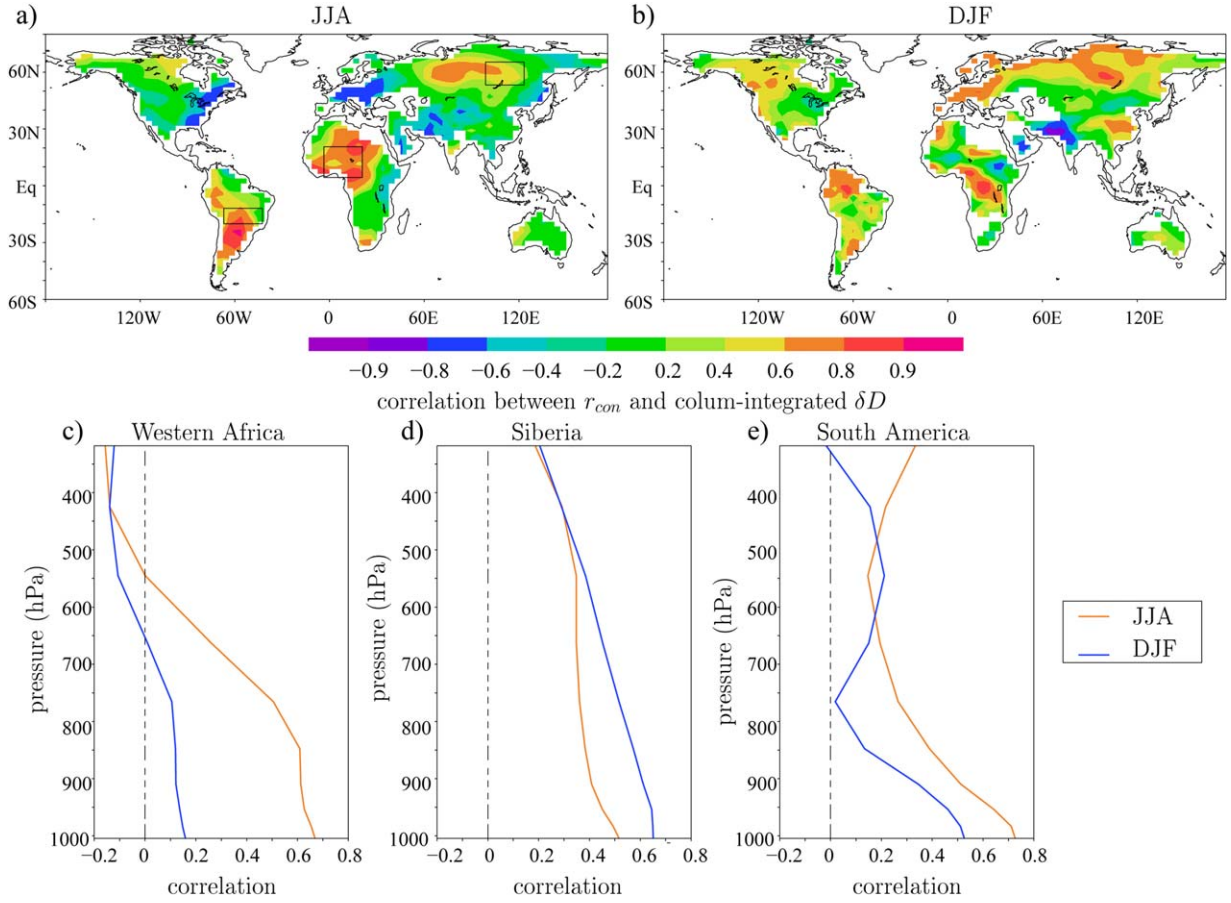


**Figure 5.** Daily correlation coefficient between  $r_{con}$  of the low-level vapor and column-integrated  $\delta D$  in (a) JJA and (b) DJF. Vertical profiles of the daily correlation coefficient between  $r_{con}$  and  $\delta D$  of the vapor at each vertical level, on average over different regions: (c) western Africa ( $10^{\circ}\text{N}$ – $20^{\circ}\text{N}$ – $0^{\circ}\text{E}$ – $20^{\circ}\text{E}$ ), (d) Siberia ( $55^{\circ}\text{N}$ – $65^{\circ}\text{N}$ – $110^{\circ}\text{E}$ – $120^{\circ}\text{E}$ ), and (e) South America ( $20^{\circ}\text{S}$ – $10^{\circ}\text{S}$ – $70^{\circ}\text{W}$ – $50^{\circ}\text{W}$ ), for different seasons JJA (orange) and DJF (blue).

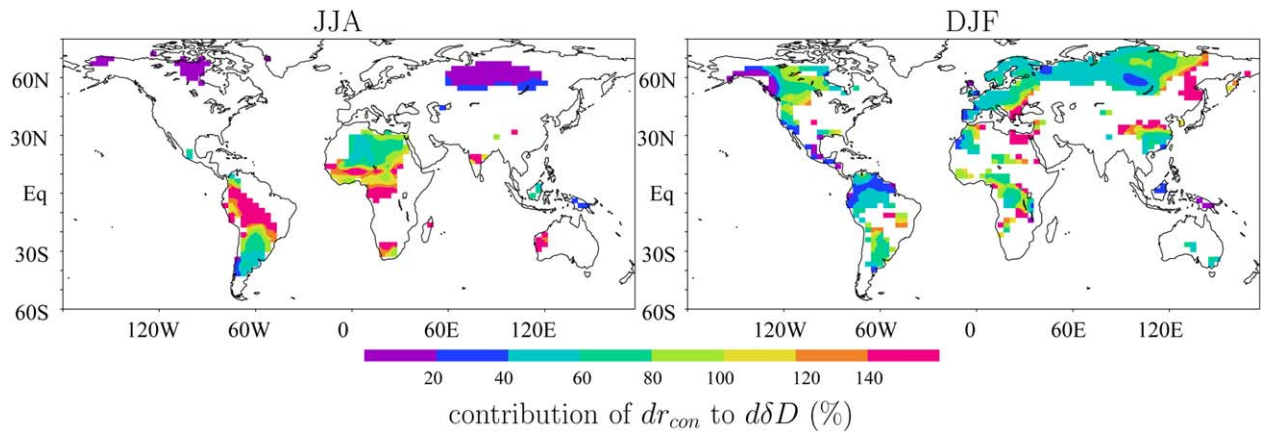


**Figure 6.** Quantitative contribution of  $r_{con}$  variations to column-integrated  $\delta D$  daily variations in (a) JJA and (b) DJF, as quantified by  $\frac{dr_{con}}{d\delta D} \cdot (\delta D_{con} - \delta D_{oce}) \cdot 100$  (see text for variable definitions). The slope  $\frac{dr_{con}}{d\delta D}$  is calculated where the correlation coefficient between  $r_{con}$  and column-integrated  $\delta D$  is greater than 0.4.



distillation predicts a linear relationship between  $\delta D$  and  $\ln(W)$ . D1\_iso shares similar spatial and seasonal patterns with D1 (Figure 7). For example, in South America and in western Africa, patterns are very similar in D1 and in D1\_iso. In these regions, as we go inland, D1 and D1\_iso both increase. This is confirmed by correlations of 0.86 and 0.97 between D1 and D1\_iso in these regions (Figures 7e and 7f).

[54] The maps in Figure 7 could be interpreted independently of continental recycling, by the combination of two effects: the distillation effect and the amount effect [Risi

*et al.*, 2010b]. When the distillation effect dominates, the drier the air in terms of  $W$ , the more depleted the vapor. This dryness could come either from cooling as air goes poleward (i.e., temperature effect, Dansgaard [1964]), or from large-scale subsidence from higher in the troposphere [Galewsky and Hurley, 2010]. This explains at least partially the positive correlations in high latitudes and dry subtropical regions. When the amount effect dominates, the more intense the convection, the more depleted the vapor, due to the depleting effect of unsaturated downdrafts, rainfall reevaporation in a moist environment and rain-vapor

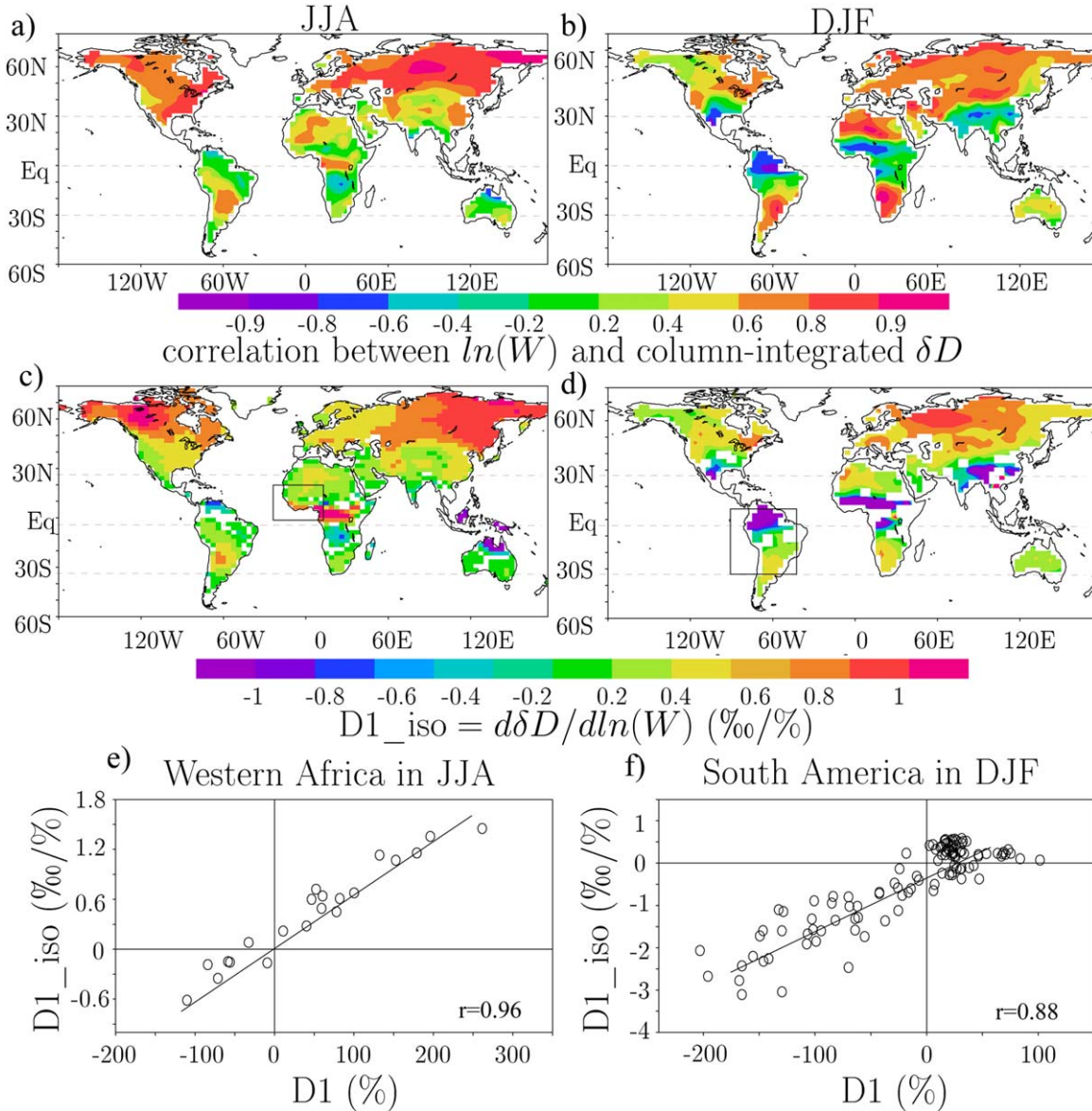


**Figure 7.** (a) Daily correlation coefficient ( $r$ ) of the linear regression between precipitable water and  $\delta D$  of total column water vapor in JJA. (b) Slope of this linear regression, where the correlation coefficient is greater than 0.2. (c and d) Same as Figures 7a and 7b but in DJF. This figure can be compared with Figure 2. Such comparison is shown as scatterplots with this example of western Africa in (e) JJA and South America in (f) DJF. These scatterplots show the slope of the linear regression between precipitable water and  $\delta D$  of total column water vapor, as a function of the slope of the linear regression between precipitable water and  $r_{con}$ , for each location in the black rectangle of the above map ( $20^{\circ}\text{W}$ – $15^{\circ}\text{E}$ – $5^{\circ}\text{N}$ – $20^{\circ}\text{N}$  for western Africa and  $90^{\circ}\text{W}$ – $30^{\circ}\text{W}$ – $30^{\circ}\text{S}$ – $10^{\circ}\text{N}$  for South America).

diffusive exchanges [Lawrence *et al.*, 2004; Risi *et al.*, 2008; Worden *et al.*, 2007; Field *et al.*, 2010]. This explains at least partially the negative correlations in convective regions.

[55] However, the resemblance between Figures 2 and 7 in many parts of the tropics suggest that over tropical land and at the intraseasonal scale, continental recycling may play a role in controlling  $\delta D$  that has been so far underestimated. Furthermore, we have shown in section 4.2 that  $r_{con}$  variations contribute quantitatively to  $\delta D$  variations. The pure distillation and amount effects can be estimated in places where D1 is zero, corresponding to the intercepts in Figures 7e and 7f. As expected, in the dry Sahel, the distillation effect leads to very slightly positive  $d\delta D/d\ln(W)$  and in the moist Amazon, the amount effect leads to negative  $d\delta D/d\ln(W)$ .

#### 4.4. Potential to Discriminate Between Sensitivity Tests

[56] In the previous section, we have shown a spatial link between D1 and D1<sub>iso</sub>. Now we check whether D1<sub>iso</sub> can discriminate between simulations differing by D1. Figure 8 shows the maps of the D1<sub>iso</sub> differences between the sensitivity tests and the control simulation. These maps share similar patterns with the corresponding maps for D1 (Figure 3). For example D1 is lower in “bare-soil” than in the control simulation, and so is D1<sub>iso</sub>, in South America in JJA and DJF, in western Africa in DJF and in southeastern Asia in DJF. D1 is higher in the “rveg” than in the control simulation, and so is D1<sub>iso</sub>, in most of South America in JJA and DJF and in most of Africa in JJA. In South America in particular, where D1 is the largest in “baresoil” compared to the control, D1<sub>iso</sub> is also the largest in “baresoil” compared to the control. The reverse holds for “rveg” (Figure 8e). This can be seen also in tropical average (Figure 8f).

[57] Figure 8f plots an observable diagnostic (D1<sub>iso</sub>) as a function of a nonobservable diagnostic (D1) which is of interest to evaluate the simulation of land-atmosphere coupling in climate models. The ultimate goal would thus be to add on this plot real observations for D1<sub>iso</sub>. This would help us constrain D1: for example, if average observed D1<sub>iso</sub> is positive, this would suggest that the “rveg” simulation, with a relatively high D1, is more realistic. Hall and Qu [2006] applied a similar approach to constrain the snow albedo feedback. However, using D1<sub>iso</sub> to constrain D1 is possible only if the observational uncertainty on D1<sub>iso</sub> is small enough compared to the simulation spread. In the next section, we check this condition.

## 5. Comparison With Data

### 5.1. Basic Annual Mean Comparison

[58] Figure 9 compares annual-mean column-integrated  $\delta D$  observed by GOSAT and TES and simulated by LMDZ after collocation and convolution by the kernels corresponding to each data set. The spatial patterns of  $\delta D$  retrieved by GOSAT and TES are very consistent with each other (Figures 9a and 9d). They both capture the decrease of  $\delta D$  with latitude and with altitude (e.g., Tibet), lower values in dry oceanic (e.g., off Peru) and continental (e.g., Sahara) regions and a local minimum over the

southeastern Asia. The spatial correlations between the two fields are 0.81 at the global scale and 0.56 in the tropics. Overall, spatial variations are smoother in TES than in GOSAT (Figures 9b and 9e): the global spatial standard deviation is 58% smaller in TES than in GOSAT (Table 3). This is partly due to the smoothing effect of TES kernels (Figures 9e and 9f), which decreases the global spatial standard deviation by 36% (Table 2).

[59] To first order, LMDZ captures well the spatial patterns for both GOSAT and TES. When collocation and convolution are applied, the correlations between simulated and observed  $\delta D$  are 0.98 globally and 0.92 in the tropics for GOSAT, and 0.95 globally and 0.90 in the tropics for TES. In all cases, the convolution with the kernels improves the correlation coefficients by 0.06 up to 0.23. Compared to both data sets, LMDZ underestimates the equatorpole gradient, consistent with the results from other data sets [Risi *et al.*, 2012a] and models [Yoshimura *et al.*, 2001; Werner *et al.*, 2011]. In addition, when compared to GOSAT, LMDZ simulates maxima over the ocean east of South America and Africa, rather than over land masses as in the data. This appears to be an artifact of the convolution, because model outputs without convolution show maxima over land masses (Figures 9b and 9c).

### 5.2. Comparison of Intraseasonal Relationships

[60] Figure 10 compares the observed and simulated daily correlations between  $\ln(W)$  and column-integrated  $\delta D$ . The main spatial patterns described in section 4.3 are found in GOSAT observations (Figures 9a and 9b), with maximum positive correlations over the dry Sahara, the southern half of South America, southern Africa, and Australia and high boreal latitudes in summer.

[61] LMDZ captures well the correlation patterns and magnitudes observed by both GOSAT and TES. Compared to GOSAT observations, LMDZ underestimates the correlation over the Sahara (consistent with Risi *et al.* [2010b]). But this underestimate is not noticeable compared to TES. Compared to both GOSAT and TES, LMDZ overestimates the negative correlations over convective regions (northern South America in DJF, Central America in JJA, and southeastern Asia in both seasons). An overestimated amount effect was also found for other models [Lee *et al.*, 2009b]. In addition, humidity biases in LMDZ lead convolved outputs to artificially feature larger negative correlations in these regions than initially simulated (supporting information).

[62] The slopes of column-integrated  $\delta D$  as a function of  $\ln(W)$  (i.e., D1<sub>iso</sub>) are compared in Figure 11, for locations where correlations are greater than 0.2 for GOSAT and than 0.1 for TES. This figure mirrors the D1<sub>iso</sub> maps of Figures 7b and 7d, in the sense that it represents the same maps but after accounting for GOSAT and TES spatio-temporal sampling and instrument sensitivity. Qualitatively, the main spatial features described in section 4.3 are captured by GOSAT and TES. Quantitatively, GOSAT exhibits larger slopes (Figures 11a–11d), about twice larger in tropical average (Table 3). Some of these differences can be attributed to different instrument sensitivities. In GOSAT, the effect of instrument sensitivity is to systematically attenuate negative slopes (supporting information). Apart from this effect, instrument sensitivity as reflected by averaging kernels are not expected to systematically distort

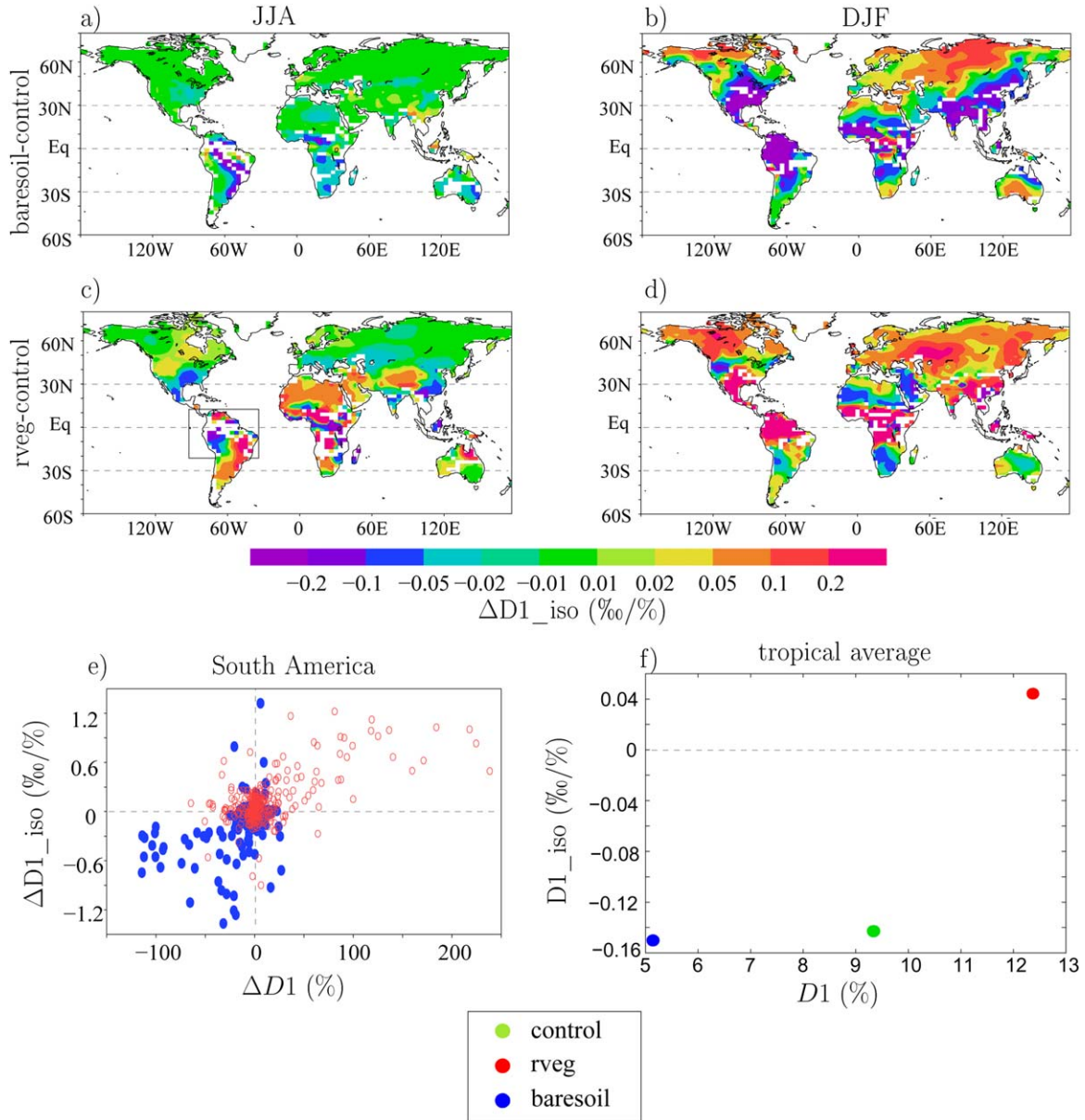


**Figure 8.** Difference between sensitivity tests and control simulation in D1<sub>iso</sub> (the slope of the linear regression between  $\ln(W)$  and column-integrated  $\delta D$ ). The sensitivity tests are (a, b) “baresoil” (less bare soil fraction) and (c, d) “rveg” (reduced stomatal resistance). Linear regression is calculated on daily time series for JJA (Figure 8a and 8c) and DJF and results are shown only when the correlation coefficient is greater than 0.2. This figure is like Figures 7b and 7e but for differences between simulations. It can be compared with Figure 3. (e) Difference between sensitivity tests and control simulation in the slope of the linear regression between  $\ln(W)$  and column-integrated  $\delta D$  (D1<sub>iso</sub>), as a function of the difference between sensitivity tests and control simulation in the slope of the linear regression between  $\ln(W)$  and  $\ln(1 - r_{con})$  (D1), at all locations in South America (20°S–15°N–90°W–30°W) black rectangle on c in DJF. (f) Same as Figure 8e but tropical mean (30°S–30°N) and average over JJA and DJF. Means are calculated over all locations and seasons where correlation coefficients are greater than 0.2 for all three simulations, to represent average over the same spatial domain for all three simulations.

$\delta D$  versus  $\ln(W)$  slopes (supporting information). Differences between TES and GOSAT in the regions of positive slopes could thus be attributed to observation biases that depend differently on  $W$  in TES and in GOSAT.

[63] When collocated and convolved with the appropriate averaging kernels, LMDZ simulates qualitatively well the spatial patterns of D1<sub>iso</sub> (Figure 11). Quantitatively, however, LMDZ underestimates D1<sub>iso</sub> compared to



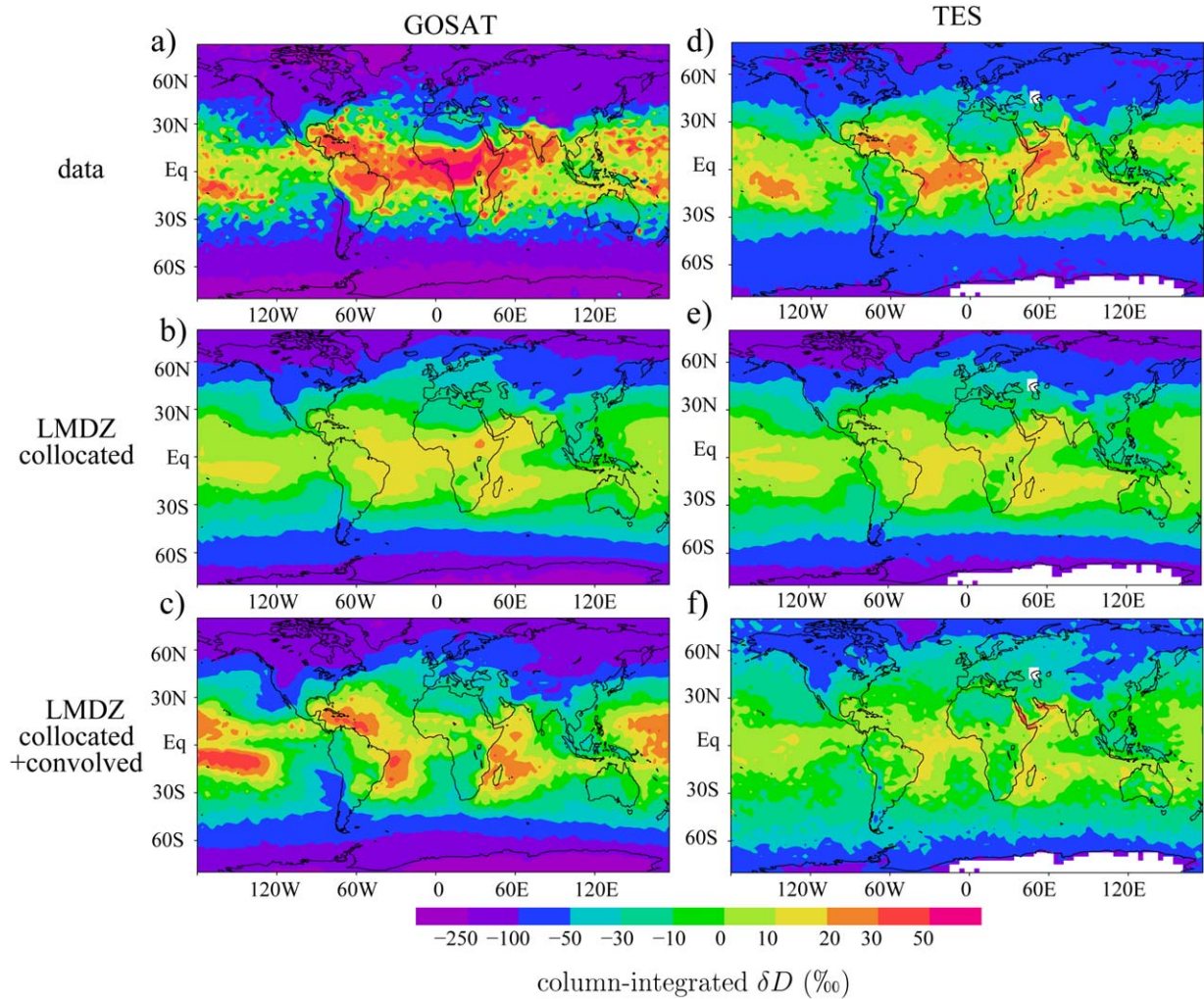


**Figure 9.** Comparison of column-integrated  $\delta D$  between (a) GOSAT observations, (b) collocated LMDZ outputs, and (c) collocated LMDZ outputs convolved with GOSAT averaging kernels. (d–f) Same as Figures 9a–9c but for comparison of column-integrated  $\delta D$  between TES and LMDZ. To focus on spatial variations in absence of absolute calibration, we subtract the mean  $\delta D$  over  $40^{\circ}\text{S}$ – $40^{\circ}\text{N}$  for each  $\delta D$  map. The spatial standard deviation at the global scale of these maps is indicated in Table 2.

both GOSAT and TES. In tropical average where observed slopes are positive, LMDZ underestimates slopes by a factor of about 2 compared to GOSAT and about 4 compared to TES (Table 3). This is due to an underestimate of both negative and positive slopes. First,

**Table 2.** Spatial Standard Deviation at the Global Scale of Column-Integrated  $\delta D$  for GOSAT and TES Observations, Collocated LMDZ Outputs, and Collocated and Convolved LMDZ Outputs<sup>a</sup>

Data Set	GOSAT	TES
Observations	114	49
Collocated LMDZ outputs	54	53
Collocated and Convolved LMDZ outputs	69	35

<sup>a</sup>LMDZ outputs are collocated and convolved to compare either with GOSAT or TES observations. All values are expressed in ‰.

LMDZ simulates negative slopes in moist tropical regions that have a greater extent than observed. In regions where observed slopes are negative, simulated slopes are also too negative. This is consistent with an overestimate of the amount effect [Lee *et al.*, 2009b]. But this could also be attributed to the effect of humidity biases: even if simulated  $\delta D$  is correct, humidity biases in LMDZ lead convolved outputs to systematically decrease negative slopes (supporting information). Second, LMDZ underestimates positive slopes in the driest regions, such as the Sahara in winter, especially compared to GOSAT. This cannot be explained by humidity biases, since humidity biases in LMDZ lead convolved outputs to systematically increase positive slopes compared to GOSAT. Therefore, although GOSAT and TES have different sensitivities to  $\delta D$ , both data sets suggest that LMDZ underestimates  $D1_{iso}$ .

**Table 3.** Comparison of the Slopes (Columns 2 and 3) of Column-Integrated  $\delta D$  as a Function  $\ln(W)$ , on Average Over JJA and DJF and Over All Tropical Land Locations, for GOSAT and TES Observations, Raw LMDZ Outputs, Collocated LMDZ Outputs, Collocated and Convolved LMDZ Outputs, and for Our Three LMDZ-ORCHIDEE Simulations<sup>a</sup>

Data Set	GOSAT	TES	GOSAT Where Observed Slopes Are Positive	TES Where Observed Slopes Are Positive	GOSAT in Western Africa in JJA	TES in Western Africa in JJA
Data	0.50	0.26	0.99	0.30	1.42	0.26
Raw LMDZ outputs	−0.24	−0.18	−0.02	−0.17	0.01	−0.04
Collocated LMDZ outputs	0.07	0.10	0.10	0.12	0.24	−0.20
Collocated and convolved LMDZ outputs	−0.05	0.04	0.43	0.07	0.76	−0.70
Raw LMDZ-ORCHIDEE control	−0.39	−0.27	−0.19	−0.24	−0.15	−0.46
Raw LMDZ-ORCHIDEE baresoil	−0.47	−0.33	−0.26	−0.30	−0.20	−0.56
Raw LMDZ-ORCHIDEE rveg	−0.33	−0.15	−0.13	−0.14	−0.23	−0.03

<sup>a</sup>Values are in %/%. Tropical land averages are calculated where the correlation coefficients for all the simulations and observations are greater than 0.1, to ensure that averages are done over the same spatial domain for all quantities that we compare. Columns 4 and 5: same as columns 2 and 3 but over tropical land points where observed slopes are positive. Columns 6 and 7: same as columns 2 and 3 but over western Africa (defined as 20°W–15°E–5°N–20°N as in Figure 5) in JJA.

[64] The suggestion that LMDZ underestimates  $D1_{iso}$  is further supported by comparison with ground-based remote-sensing measurements of column-integrated  $\delta D$  (not shown). We selected four TCCON sites [Wunch *et al.*, 2011] and two MUSICA sites [Schneider *et al.*, 2010a, 2010b] that lie over land and with a significant continental influence: Park Falls, Lamont and Pasadena (United States), Bremen (Germany) for TCCON and Jungfraujoch (Switzerland), Karlsruhe (Germany) for MUSICA. After convolution with appropriate averaging kernels [Risi *et al.*, 2012a], LMDZ underestimate  $D1_{iso}$  at all sites and for both JJA and DJF, except at Karlsruhe in JJA. Therefore, almost all available data sets suggest that LMDZ underestimates  $D1_{iso}$ .

### 5.3. Implications for Model Evaluation of the Role of Continental Recycling

[65] The fact that LMDZ underestimates  $D1_{iso}$  compared to both GOSAT and TES suggests that LMDZ underestimates the role of continental recycling in intraseasonal variations of continental moisture. On average over tropical land points, LMDZ-ORCHIDEE simulates  $D1_{iso}$  values that are even lower than in stand-alone LMDZ (Table 3). This suggests that the coupling with ORCHIDEE weakens the role of continental recycling on the intraseasonal variability of continental moisture. This can be explained by the fact that in ORCHIDEE, transpiration has access to a deeper reservoir of soil moisture that fluctuates at a lower frequency. Therefore, the presence of vegetation in ORCHIDEE smoothes the evapo-transpiration variations. In ORCHIDEE, increasing the sensitivity of evapo-transpiration to soil moisture may improve the model-data agreement (section 3.3).

[66] An important caveat of our approach is that  $D1_{iso}$  may not only reflect the role of continental recycling. As discussed in section 4.3, the distillation and amount effects may also play a role. If we find that in a model simulation, the slope is too low, how can we ensure that this is only due to the underestimated role of continental recycling? It may also be due to the distillation effect which is not efficient enough (e.g., excessive diffusion: Risi *et al.* [2012b]), or because the depleting effect of convection is too strong (e.g., excessively strong unsaturated downdrafts). An idea

could be to compare  $D1_{iso}$  over land versus ocean, assuming that the distillation and convection effects over land and ocean would be the same. But it would not be conclusive either because convection over land and ocean has a different character [Zipser and LeMone, 1980; Nesbitt and Zipser, 2003; Liu and Zipser, 2005].

[67] In section 4.2, we showed that in western Africa in both seasons, in the Congo basin in DJF and in South America in JJA, simulated  $\delta D$  variations were mainly caused by  $r_{con}$  variations. This suggests that in this regions we may have more confidence that the underestimate of  $D1_{iso}$  (Table 3) can be interpreted as an underestimate of the role of continental recycling.

## 6. Conclusions

[68] In this paper, we design a water-tagging-based diagnostic, named  $D1$ , to estimate the role of continental recycling on the intraseasonal variability of continental moisture and precipitation. Consistent with previous studies [e.g., Schär *et al.*, 1999], we show that this role is limited in coastal regions, in Europe and in the United States, where the intraseasonal variability of continental moisture is mainly driven by variability in moisture convergence bringing mainly oceanic precipitation. However, on deeper continental interiors (e.g., Siberia) and in tropical land regions where the continental recycling is strong (e.g., southern America, Congo basin), the role of continental recycling on the intraseasonal variability of continental moisture becomes important. We show that this role is sensitive to model parameter choice, for example, those modulating the relationship between soil-water content and evapo-transpiration. We aim at proposing an observational constrain for the simulation of this role.

[69] We show that low-level  $\delta D$  is a good tracer for variability in continental recycling at the intraseasonal scale, due to the enriched signature of transpiration. We show that over land regions, the relationship between column-integrated  $\delta D$  and the logarithm of precipitable water, named  $D1_{iso}$ , is a good observable proxy for  $D1$  in several regions, in particular in western Africa, in the Congo basin and in South America. This proxy could help



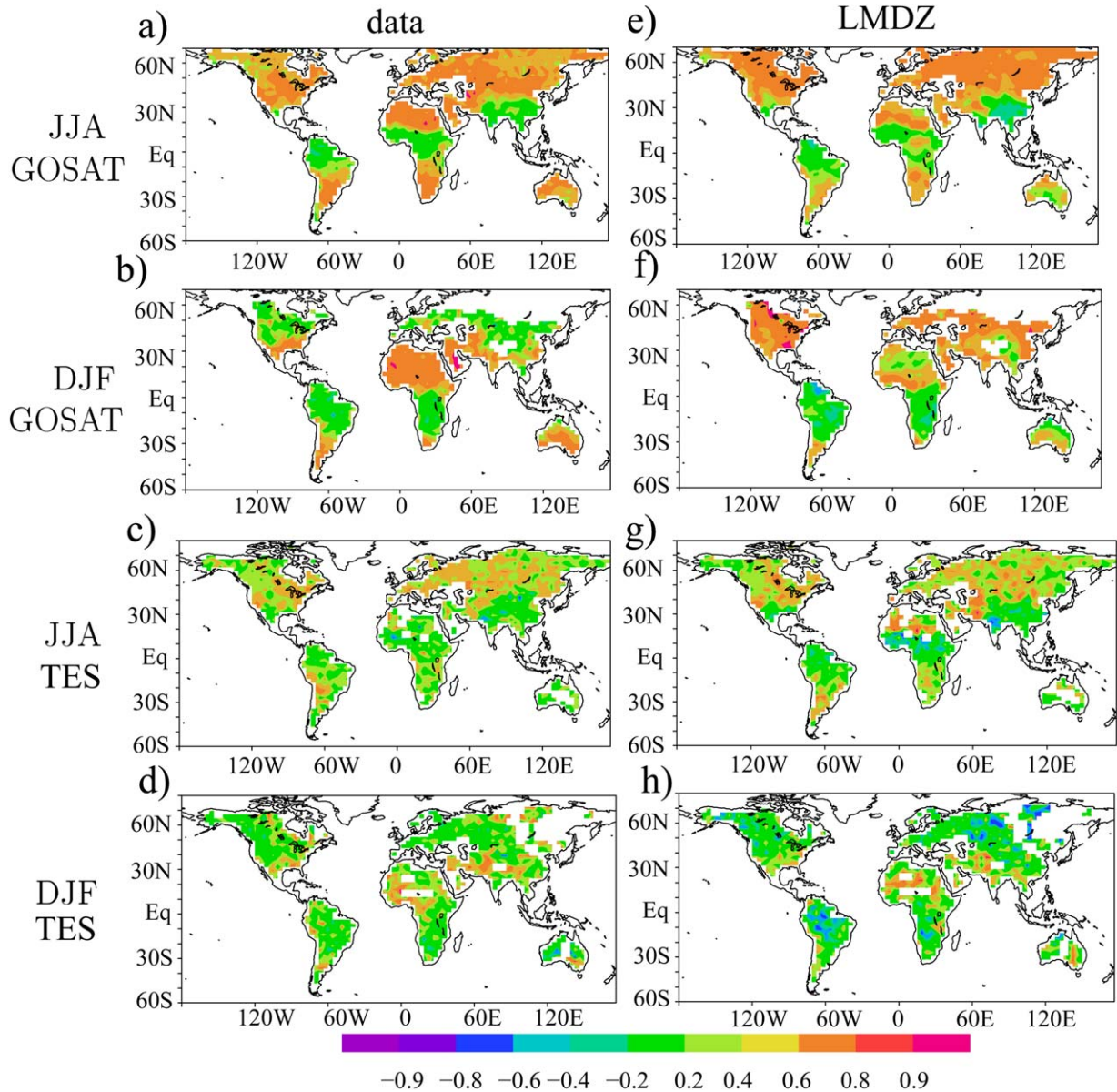


**Figure 10.** Correlation coefficient for the relationship of column-integrated  $\delta D$  as a function of  $\ln(W)$ , for (a, b) GOSAT observations, for the (c, d) TES data, for (e, f) LMDZ outputs after collocation and convolution by GOSAT kernels, and for (g, h) LMDZ outputs after collocation and convolution by TES kernels. Results are shown for both JJA and DJF.

discriminate between different simulations to select the one with the most realistic role of continental recycling on the intraseasonal variability of continental moisture.

[70] We test this possibility with two satellite data sets: GOSAT and TES. Compared to both data sets, LMDZ underestimates  $D1_{iso}$ . This suggests that LMDZ underestimates the role of continental recycling on the intraseasonal variability of continental moisture. However, a doubt subsists whether other misrepresentation of atmospheric processes independent of continental recycling (e.g., convection, large-scale circulation) may also contribute to this underestimate. The respective role of continental recycling

and atmospheric processes on water vapor isotopic composition need to be more accurately quantified and understood, before we can practically use isotopic data to evaluate models in terms of continental recycling. This requires a more detailed model analysis and a more careful evaluation against isotopic measurements.

[71] Finally, the different sensitivity between GOSAT and TES calls for more calibration and cross-validation studies which would not only focus on mean  $\delta D$  [e.g., Worden *et al.*, 2010] but also on  $\delta D$  variations. The development of in situ measurements [e.g., Gupta *et al.*, 2009; Lee *et al.*, 2007b; Welp *et al.*, 2012], on the ground or onboard



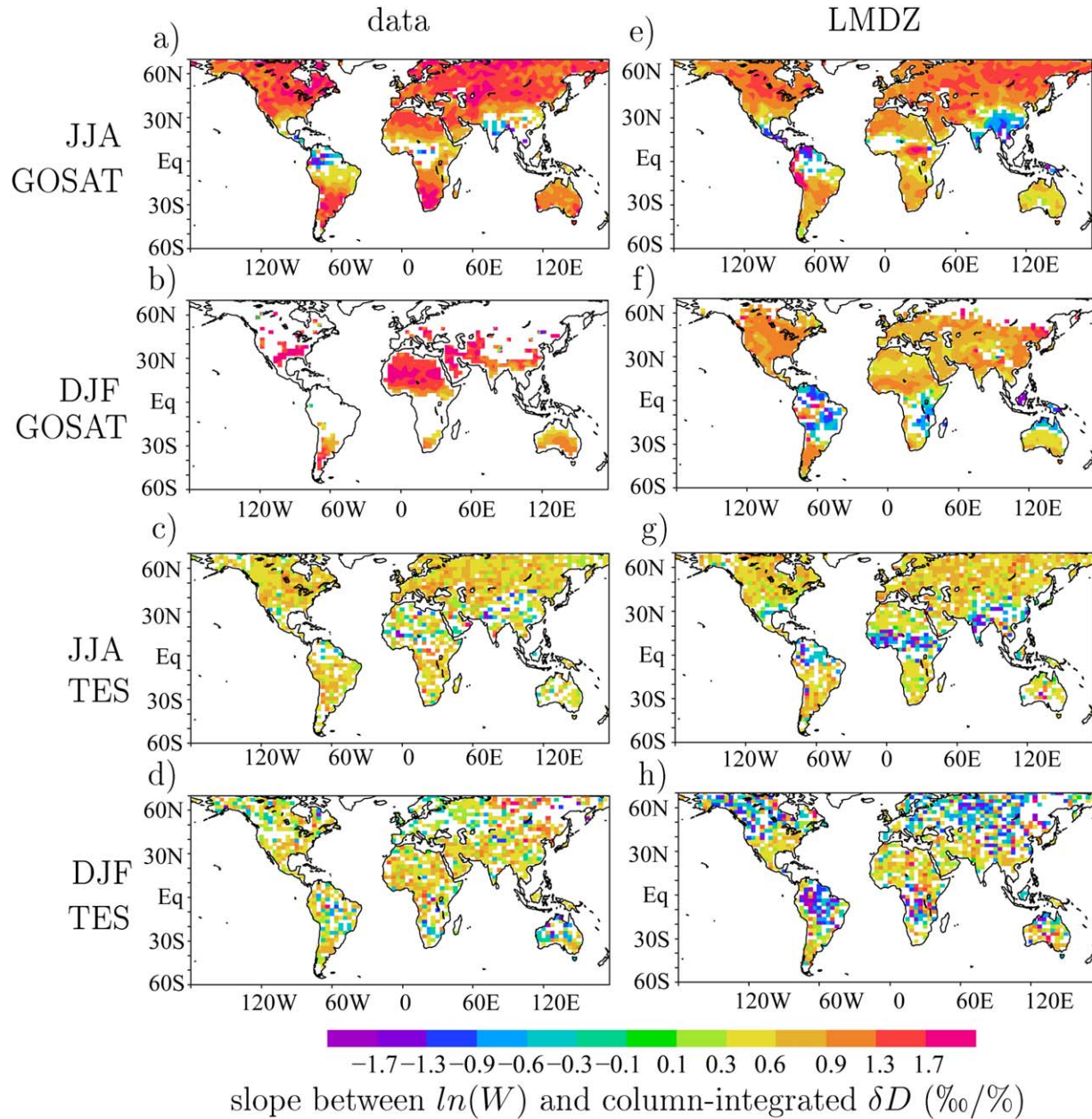


**Figure 11.** Same as Figure 10 but for slopes (i.e.,  $D1_{iso}$ ) instead of correlation coefficients. Slopes are plotted where correlation coefficients are greater than 0.2. The average over all tropical land points of these slopes are indicated in Table 3.

aircrafts, will offer more validation opportunities for satellite data sets and models.

[72] **Acknowledgments.** LMDZ and LMDZ-ORCHIDEE simulations were performed on the NEC supercomputer of the IDRIS computing center. We thank Matthias Schneider and two anonymous reviewers for their constructive comments during the review process.

## References

- Barnes, C., and G. Allison (1988), Tracing of water movement in the unsaturated zone using stable isotopes of hydrogen and oxygen, *J. Hydrol.*, **100**, 143–176.
- Beljaars, A., P. Viterbo, M. J. Miller, and A. K. Betts (1996), The anomalous rainfall over the united states during July 1993: Sensitivity to land surface parameterization and soil moisture anomalies, *Mon. Weather Rev.*, **124**, 362–383.
- Betts, A. K. (1992), Fife atmospheric boundary layer budget methods, *J. Geophys. Res.*, **97**, D18, 18,523–18,532.
- Betts, A. K. (2004), Understanding hydrometeorology using global models, *Bull. Am. Meteorol. Soc.*, **85**(11), 1673–1688, doi:10.1175/BAMS-85-11.
- Boesch, H., N. M. Deutscher, T. Warneke, K. Byckling, A. J. Cogan, D. W. T. Griffith, J. Notholt, R. J. Parker, and Z. Wang, (2012), HDO/H<sub>2</sub>O ratio retrievals from GOSAT, *Atmos. Meas. Tech. Discuss.*, **5**, 5, 6643–6677, doi:10.5194/amtd-5-6643-2012.
- Bony, S., C. Risi, and F. Vimeux (2008), Influence of convective processes on the isotopic composition ( $\delta^{18}O$  and  $\delta^2H$ ) of precipitation and water vapor in the Tropics. Part 1: Radiative-convective equilibrium and TOGA-COARE simulations, *J. Geophys. Res.*, **113**, D19305, doi:10.1029/2008JD009942.

- Bosilovich, M. G., and S. D. Schubert (2002), Water vapor tracers as diagnostics of the regional hydrologic cycle, *J. Hydrometeorol.*, **3**, 149–165.
- Braud, I., T. Bariac, P. Biron, and M. Vauclin (2009a), Isotopic composition of bare soil evaporated water vapor, Part II: Modeling of RUBIC IV experimental results, *J. Hydrol.*, **369**, 17–29.
- Braud, I., P. Biron, T. Bariac, P. Richard, L. Canale, J. Gaudet, and M. Vauclin (2009b), Isotopic composition of bare soil evaporated water vapor. Part I: RUBIC IV experimental setup and results, *J. Hydrol.*, **369**, 1–16.
- Bretherton, C. S., M. E. Peters, and L. E. Back (2004), Relationships between water vapor path and precipitation over the tropical oceans, *J. Clim.*, **17**, 1517–1528.
- Brown, D., J. Worden, and D. Noone (2008), Comparison of atmospheric hydrology over convective continental regions using water vapor isotope measurements from space, *J. Geophys. Res.*, **113**, D15124, doi:10.1029/2007JD009676.
- Brubaker, K. L., D. Entekhabi, and P. Eagleson (1993), Estimation of continental precipitation recycling, *J. Clim.*, **6**, 1077–1099.
- Brubaker, K., D. Entekhabi, and P. Eagleson (1994), Atmospheric water-vapor transport and continental hydrology over the America, *J. Hydrol.*, **155**, 407–428.
- Budyko (1974), *Climate and Life*, Elsevier, New York.
- Burde, G. I., A. Zangvil, and P. J. Lamb (1996), Estimating the role of local evaporation in precipitation for a two-dimensional region, *J. Clim.*, **9**, 1328–1338.
- Choisnel, E., S. V. Jourdain, and C. J. Jaquart (1995), Climatological evaluation of some fluxes of the surface energy and soil water balances over France, *Ann. Geophys.*, **13**, 666–674.
- Cook, B. I., B. B. Gordon, and S. Levis (2006), Soil moisture feedbacks to precipitation in southern Africa, *J. Clim.*, **19**, 4198–4206.
- Craig, H., and L. I. Gordon (1965), Deuterium and oxygen-18 variations in the ocean and marine atmosphere, in *Stable Isotopes in Oceanographic Studies and Paleotemperatures*, pp. 9–130, Laboratorio di Geologia Nucleare, Pisa, Italy.
- Dansgaard (1964), Stable isotopes in precipitation, *Tellus*, **16**, 436–468.
- de Ridder, K. (1997), Land surface processes and the potential for convective precipitation, *J. Geophys. Res.*, **102**, D25, 30,085–30,090.
- de Rosnay, P., M. Brien, and J. Polcher (2000), Sensitivity of the surface fluxes to the number of layers in the soil model used in GCMs, *Geophys. Res. Lett.*, **27**(20), 3329–3332.
- Dirmeyer, P. A., and K. L. Brubaker (1999), Contrasting evaporative moisture sources during the drought of 1988 and the flood of 1993, *J. Geophys. Res.*, **104**(D16), 19,383–19,397.
- Dirmeyer, P. A., and K. L. Brubaker (2007), Characterization of the global hydrologic cycle from a back-trajectory analysis of atmospheric water vapor, *J. Hydrometeorol.*, **8**(1), 20–37, doi:10.1175/JHM557.1.
- Dirmeyer, P. A., C. A. Schlosser, and K. L. Brubaker (2008), Precipitation, recycling, and land memory: An integrated analysis, *J. Hydrometeorol.*, **10**, 278–288.
- Dirmeyer, P. A., K. L. Brubaker, and T. DelSole (2009), Import and export of atmospheric water vapor between nations, *J. Hydrol.*, **365**(1–2), 12–12, doi:10.1016/j.jhydrol.2008.11.016.
- d'Odorico, P., and A. Porporato (2004), Preferential states in soil moisture and climate dynamics, *Proc. Natl. Acad. Sci.*, **101**(24), 8848–8851, doi:10.1073/pnas.0401428101.
- Dominguez, F., and P. Kumar (2008), Precipitation recycling variability and ecoclimatological stability – A study using NARR data. Part I: Central U.S. Plains ecoregion, *J. Clim.*, **21**:5165–5186, http://dx.doi.org/10.1175/2008JCLI1756.1.
- Dominguez, F., P. Kumar, X. Liang, and M. Ting (2006), Impact of atmospheric moisture storage on precipitation recycling, *J. Clim.*, **19**(8), 1513–1530, doi:10.1175/JCLI3691.1.
- Dominguez, F., P. Kumar, and E. R. Vivoni (2008), Precipitation recycling variability and ecoclimatological stability? A study using NARR data. Part II: North American Monsoon Region, *J. Clim.*, **21**, 5187–5203.
- d'Orgeval, T. (2006), Impact du changement climatique sur le cycle de l'eau en Afrique de l'Ouest: Modélisation et incertitudes. PhD thesis, Univ. Paris 6.
- Ducoudré, N., K. Laval, and A. Perrier (1993), SECHIBA, a new set of parametrizations of the hydrological exchanges at the land-atmosphere interface within the LMD atmospheric general circulation model, *J. Clim.*, **6**, 248–273.
- Duffourg, F., and V. Ducrocq (2011), Origin of the moisture feeding the heavy precipitating systems over southeastern France, *Nat. Hazards Earth Syst. Sci.*, **11**(4), 1163–1178.
- Dufresne, J.-L., et al. (2012), Climate change projections using the IPSL-CM5 earth system model: From CMIP3 to CMIP5, *Clim. Dyn.*, **40**(9–10), 1–43, doi:10.1007/s00382-012-1636-1.
- Ek, M. B., and A. A. M. Holtslag (2004), Influence of soil moisture on boundary layer cloud development, *J. Hydrometeorol.*, **5**, 86–99.
- Eltahir, E. A. B., and R. L. Bras (1994), Precipitation recycling in the Amazon basin, *Q. J. R. Meteorol. Soc.*, **120**(518), 861–880, doi:10.1002/qj.49712051806.
- Eltahir, E. A. B., and R. L. Bras (1996), Precipitation recycling, *Rev. Geophys.*, **34**(3), 367–378.
- Entekhabi, D., I. Rodriguez-Iturbe, and R. L. Bras (1992), Variability in large-scale water balance with land surface-atmosphere interaction, *J. Clim.*, **5**, 798–813.
- Ferguson, C. R., and E. F. Wood (2011), Observed land-atmosphere coupling from satellite remote-sensing and re-analysis, *J. Hydrometeorol.*, **12**, 1221–1254, http://dx.doi.org/10.1175/2011JHM1380.1.
- Ferguson, C. R., E. F. Wood, and R. K. Vinukollu (2012), A global inter-comparison of modeled and observed land-atmosphere coupling, *J. Hydrometeorol.*, **13**, 749–784, http://dx.doi.org/10.1175/JHM-D-11-0119.1.
- Field, R. D., D. B. A. Jones, and D. P. Brown (2010), The effects of post-condensation exchange on the isotopic composition of water in the atmosphere, *J. Geophys. Res.*, **115**, D24305, doi:10.1029/2010JD014334.
- Findell, K. L., and E. A. B. Eltahir (2003a), Atmospheric controls on soil moisture-boundary layer interactions. Part I: Framework development, *J. Hydrometeorol.*, **4**, 552–569.
- Findell, K. L., and E. A. B. Eltahir (2003b), Atmospheric controls on soil moisture? Boundary layer interactions. Part II: Feedbacks within the continental United States, *J. Hydrometeorol.*, **4**, 570–583.
- Fischer, E. M., S. I. Seneviratne, D. Lüthi, and C. Schär (2007), Contribution of land-atmosphere coupling to recent European summer heat waves, *Geophys. Res. Lett.*, **34**, L06707, doi:10.1029/2006GL029068.
- Flanagan, L. B., and J. R. Ehleringer (1991), Stable isotope composition of stem and leaf water: Applications to the study of plant use, *Funct. Ecol.*, **5**(2), 270–277.
- Frankenberg, C., et al. (2009), Dynamic processes governing lower-tropospheric HDO/H<sub>2</sub>O ratios as observed from space and ground, *Science*, **325**, 1374–1377.
- Frankenberg, C., D. Wunch, G. Toon, C. Risi, R. Scheepmaker, Lee, J.-E., and J. Worden (2012), Water vapor isotopologues retrievals from high resolution GOSAT short-wave infrared spectra, *Atmos. Chem. Phys. Discuss.*, **5**, 6357–6386, doi:10.5194/amtd-5-6357-2012.
- Galewsky, J., and J. V. Hurlley (2010), An advection-condensation model for subtropical water vapor isotopic ratios, *J. Geophys. Res.*, **115** (D16), D16115, doi:10.1029/2009JD013651.
- Gat, J. R. (1996), Oxygen and hydrogen isotopes in the hydrologic cycle, *Annu. Rev. Earth Planet. Sci.*, **24**, 225–262.
- Gat, J. R., and E. Matsui (1991), Atmospheric water balance in the Amazon basin: An isotopic evapotranspiration model, *J. Geophys. Res.*, **96**, 13,179–13,188.
- Gates, W. L. (1992), AMIP: The atmospheric model intercomparison project, *Bull. Am. Meteorol. Soc.*, **73**, 1962–1970.
- Gimeno, L., A. Drumond, R. Nieto, R. M. Trigo, and A. Stohl (2010), On the origin of continental precipitation, *Geophys. Res. Lett.*, **37**, L13804, doi:10.1029/2010GL043712.
- Gimeno, L., A. Stohl, R. M. Trigo, F. Dominguez, K. Yoshimura, L. Yu, A. Drumond, A. M. Duran-Quesada, and R. Nieto (2012), Oceanic and terrestrial sources of continental precipitation, *Rev. Geophys.*, **50**, RG4003, doi:10.1029/2012RG000389.
- Goessling, H. F., and C. H. Reick (2011), What do moisture recycling estimates tell us? Exploring the extreme case of non-evaporating continents, *Hydrol. Earth Syst. Sci.*, **15**, 3217–3225.
- Gong, C., and E. Eltahir (1996), Sources of moisture for rainfall in West Africa, *Water Resour. Res.*, **10**, 3115–3121.
- Guimberteau, M., K. Laval, A. Perrier, and J. Polcher (2012), Global effect of irrigation and its impact on the onset of the Indian summer monsoon, *Clim. Dyn.*, **39**(6), 1329–1348, doi:10.1007/s00382-011-1252-5.
- Guo, Z., et al. (2006), GLACE: The global land-atmosphere coupling experiment. Part II: Analysis, *J. Hydrometeorol.*, **7**(4), 611–625, doi:10.1175/JHM511.1.
- Gupta, P., D. Noone, J. Galewsky, C. Sweeney, and B. H. Vaughn (2009), Demonstration of high-precision continuous measurements of water vapor isotopologues in laboratory and remote field deployments using wavelength-scanned cavity ring-down spectroscopy (WS-CRDS) technology, *Rapid Commun. Mass Spectrom.*, **23**, 2534–2542.
- Hall, A., and X. Qu (2006), Using the current seasonal cycle to constrain snow albedo feedback in future climate change, *Geophys. Res. Lett.*, **33**, L03502, doi:10.1029/2005GL025127.



- Hoffmann, G., M. Werner, and M. Heimann (1998), Water isotope module of the ECHAM atmospheric general circulation model: A study on time-scales from days to several years, *J. Geophys. Res.*, **103**, 16,871–16,896.
- Hohenegger, C., P. Brockhaus, C. Bretherton, and C. Schär (2009), The soil moisture-precipitation feedback in simulations with explicit and parameterized convection, *J. Clim.*, **22**, 5003–5020.
- Hourdin, F., et al. (2006), The LMDZ4 general circulation model: Climate performance and sensitivity to parameterized physics with emphasis on tropical convection, *Clim. Dyn.*, **27**, 787–813.
- Joussaume, S., J. Jouzel, and R. Sadourny (1984), A general circulation model of water isotope cycles in the atmosphere, *Nature*, **311**, 24–29.
- Jouzel, J., R. D. Koster, R. J. Suozzo, G. L. Russel, J. W. C. White, and W. S. Broecker (1987), Simulations of the HDO and H<sub>2</sub>O<sub>18</sub> atmospheric cycles using the NASA GISS General Circulation Model: The seasonal cycle for present day conditions, *J. Geophys. Res.*, **92**, 14,739–14,760.
- Jouzel, J., R. Koster, R. Suozzo, G. Russell, J. White, and W. Broecker (1991), Simulations of the HDO and H<sub>2</sub>O-18 atmospheric cycles using the NASA GISS general circulation model: Sensitivity experiments for present-day conditions, *J. Geophys. Res.*, **96**, 7495–7507.
- Kleidon, A., and M. Heimann (2000), Assessing the role of deep rooted vegetation in the climate system with model simulations: Mechanism, comparison to observations and implications for Amazonian deforestation, *Clim. Dyn.*, **16**, 183–199.
- Koster, R., J. Jouzel, R. Suozzo, G. Russell, W. Broecker, D. Rind, and P. Eagleson (1986), Global sources of local precipitation as determined by the NASA/GISS GCM, *Geophys. Res. Lett.*, **13**(2), 121–124, doi:10.1029/GL013i002p00121.
- Koster, R. D., P. A. Dirmeyer, A. N. Hahmann, R. Ijpelaar, L. Tyahla, P. Cox, and M. J. Suarez (2002), Comparing the degree of land-atmosphere interaction in four atmospheric general circulation models, *J. Hydrometeorol.*, **3**, 363–375.
- Koster, R. D., et al. (2004), Regions of strong coupling between soil moisture and precipitation, *Science*, **305**, 1138–1140, doi:10.1126/science.1100217.
- Koster, R. D., et al. (2006), GLACE: The global land-atmosphere coupling experiment. Part I: Overview, *J. Hydrometeorol.*, **7**, 590–610.
- Krinner, G., N. Viovy, de Noblet-Ducoudré, N., J. Ogée, J. Polcher, P. Friedlingstein, P. Ciais, S. Sitch, and I. C. Prentice (2005), A dynamic global vegetation model for studies of the coupled atmosphere-biosphere system, *Global Biogeochem. Cycles*, **19**, GB1015, doi:10.1029/2003GB002199.
- Kurita, N., N. Yoshida, G. Inoue, and E. A. Chayanova (2004), Modern isotope climatology of Russia: A first assessment, *J. Geophys. Res.*, **109**, D03102, doi:10.1029/2003jd004046.
- Lawrence, D. M., and J. Slingo (2005), Weak land-atmosphere coupling strength in hadAM3: The role of soil moisture variability, *J. Hydrometeorol.*, **6**(5), 670–680.
- Lawrence, J. R., S. D. Gedzelman, D. Dexheimer, H.-K. Cho, G. D. Carrie, R. Gasparini, C. R. Anderson, K. P. Bowman, and M. I. Biggerstaff (2004), Stable isotopic composition of water vapor in the tropics, *J. Geophys. Res.*, **109**:D06115, doi:10.1029/2003JD004046.
- Lee, E., T. N. Chase, R. Balaji, R. G. Barry, T. W. Biggs, and P. J. Lawrence (2009a), Effects of irrigation and vegetation activity on early Indian summer monsoon variability, *Int. J. Climatol.*, **29**(4), 573–581.
- Lee, J.-E., and I. Fung (2008), “Amount effect” of water isotopes and quantitative analysis of post-condensation processes, *Hydrol. Process.*, **22**(1), 1–8.
- Lee, J.-E., I. Fung, DePaolo, D., and C. C. Fennig (2007a), Analysis of the global distribution of water isotopes using the NCAR atmospheric general circulation model, *J. Geophys. Res.*, **112**, D16306, doi:10.1029/2006JD007657.
- Lee, J.-E., B. R. Lintner, J. D. Neelin, X. Jiang, P. Gentine, C. K. Boyce, B. F. Joshua, J. T. Perron, T. L. Kubar, J. Lee, and J. Worden (2012), Reduction of tropical land region precipitation variability via transpiration, *Geophys. Res. Lett.*, **39**, L19704, doi:10.1029/2012GL053417.
- Lee, J.-E., R. Pierrehumbert, A. Swann, and B. R. Lintner (2009b), Sensitivity of stable water isotopic values to convective parameterization schemes, *Geophys. Res. Lett.*, **36**, L23801, doi:10.1029/2009GL040880.
- Lee, X., K. Kim, and R. Smith (2007b), Temporal variations of the 18O/16O signal of the whole-canopy transpiration in a temperate forest, *Global Biogeochem. Cycles*, **21**, GB3013, doi:10.1029/2006GB002871.
- Lintner, B. R., P. Gentine, K. L. Findell, F. D’Andrea, A. H. Sobel, and G. D. Salvucci (2012), An idealized prototype for large-scale land atmosphere coupling, *J. Clim.*, **26**, 2379–2389, http://dx.doi.org/10.1175/JCLI-D-11-00561.1.
- Liu, C., and E. J. Zipser (2005), Global distribution of convection penetrating the tropical tropopause, *J. Geophys. Res.*, **110**, D23104, doi:10.1029/2005JD006603.
- Marti, O., et al. (2005), The new IPSL climate system model: IPSL-CM4. Tech. Rep., Note of the Modeling Pole of IPSL, 26: 1–86.
- Mathieu, R., and T. Bariac (1996), A numerical model for the simulation of stable isotope profiles in drying soils, *J. Geophys. Res.*, **101**(D7), 12,685–12,696.
- McDonald, J. E. (1962), The evaporation-precipitation fallacy, *Weather*, **17**(5), 168–177.
- Meehl, G. A., K. Covey, T. Delworth, M. Latif, B. McAvaney, J. F. B. Mitchell, R. J. Stouffer, and K. Taylor (2007), The WCRP CMIP3 multi-model dataset: A new era in climate change research, *Bull. Am. Meteorol. Soc.*, **7**, 1383–1394.
- Milly, P. C. D. (1992), Potential evaporation and soil moisture in general circulation models, *J. Clim.*, **5**, 209–226, http://dx.doi.org/10.1175/1520-0442.
- Nesbitt, S. W., and E. J. Zipser (2003), The diurnal cycle of rainfall and convective intensity according to three years of TRMM measurements, *J. Clim.*, **16**(10), 1456–1475.
- Nicholson, S. E. (2000), Land surface processes and Sahel climate, *Rev. Geophys.*, **38**, 117–139.
- Noone, D., and I. Simmonds (2002), Associations between delta18O of water and climate parameters in a simulation of atmospheric circulation for 1979–95, *J. Clim.*, **15**, 3150–3169.
- Noone, D., et al. (2012), Factors controlling moisture in the boundary layer derived from tall tower profiles of water vapor isotopic composition following a snowstorm in Colorado, *Atmos. Chem. Phys. Discuss.*, **12**, 16,327–16,375, doi:10.5194/acpd-12-16327-2012.
- Numaguti, A. (1999), Origin and recycling processes of precipitating water over the Eurasian continent: Experiments using an atmospheric general circulation model, *J. Geophys. Res.*, **104**, 1957–1972, doi:10.1029/1998JD00026.
- Pal, J. S., and E. A. B. Eltahir (2001), Pathways relating soil moisture conditions to future summer rainfall within a model of the land-atmosphere system, *J. Clim.*, **14**, 1227–1242.
- Porporato, A. (2009), Atmospheric boundary-layer dynamics with constant bowen ratio, *Boundary Layer Meteorol.*, **132**(2), 227–240, doi:10.1007/s10546-009-9400-8.
- Raymond, D. J. (2000), Thermodynamic control of tropical rainfall, *J. R. Meteorol. Soc.*, **126**, 889–898.
- Risi, C. (2009), Les isotopes stables de l’eau: Applications l’étude du cycle de l’eau et des variations du climat, PhD thesis, Univ. Pierre Marie Curie.
- Risi, C., S. Bony, and F. Vimeux (2008), Influence of convective processes on the isotopic composition (O18 and D) of precipitation and water vapor in the tropics: Part 2: Physical interpretation of the amount effect, *J. Geophys. Res.*, **113**, D19306, doi:10.1029/2008JD009943.
- Risi, C., S. Bony, F. Vimeux, M. Chong, and L. Descroix (2010a), Evolution of the water stable isotopic composition of the rain sampled along Sahelian squall lines, *Q. J. R. Meteorol. Soc.*, **136**(S1), 227–242.
- Risi, C., S. Bony, F. Vimeux, C. Frankenberg, and D. Noone (2010b), Understanding the Sahelian water budget through the isotopic composition of water vapor and precipitation, *J. Geophys. Res.*, **115**, D24110, doi:10.1029/2010JD014690.
- Risi, C., S. Bony, F. Vimeux, and J. Jouzel (2010c), Water stable isotopes in the LMDZ4 general circulation model: Model evaluation for present day and past climates and applications to climatic interpretation of tropical isotopic records, *J. Geophys. Res.*, **115**, D12118, doi:10.1029/2009JD013255.
- Risi, C., et al. (2012a), Process-evaluation of tropical and subtropical tropospheric humidity simulated by general circulation models using water vapor isotopic observations. Part 1: Model-data intercomparison, *J. Geophys. Res.*, **117**, D05303, doi:10.1029/2011JD016621.
- Risi, C., et al. (2012b), Process-evaluation of tropical and subtropical tropospheric humidity simulated by general circulation models using water vapor isotopic observations. Part 2: An isotopic diagnostic of the mid and upper tropospheric moist bias, *J. Geophys. Res.*, **117**, D05304, doi:10.1029/2011JD016623.
- Rodriguez-Iturbe, I., D. Entekhabi, and R. L. Bras (1991a), Nonlinear dynamics of soil-moisture at climate scales: 1. Stochastic-analysis, *Water Resour. Res.*, **27**(8), 1899–1906.
- Rodriguez-Iturbe, I., D. Entekhabi, Lee, J.-S., and R. L. Bras (1991b), Non-linear dynamics of soil moisture at climate scales: 2. Chaotic analysis, *Water Resour. Res.*, **27**(8), 1907–1915.
- Rowntree, P. R., and J. A. Bolton (1983), Simulation of the atmospheric response to soil moisture anomalies over Europe, *Q. J. R. Meteorol. Soc.*, **109**(461), 501–526.



- Saeed, F., S. Hagemann, and D. Jacob (2009), Impact of irrigation on the south Asian monsoon, *Geophys. Res. Lett.*, **36**, L20711, doi:10.1029/2009GL040625.
- Salati, E., A. Dall'Olio, E. Matsui, and J. Gat (1979), Recycling of water in the Amazon basin: An isotopic study, *Water Resour. Res.*, **15**, 1250–1258.
- Santanello, J. A., C. D. Peters-Lidard, S. V. Kumar, C. Alonge, and W.-K. Tao (2009), A modeling and observational framework for diagnosing local land–atmosphere coupling on diurnal time scales, *J. Hydrometeorol.*, **10**, 577–599, doi:10.1175/2009JHM1066.1.
- Santanello, J. A., C. D. Peters-Lidard, and S. V. Kumar (2011), Diagnosing the sensitivity of local land? Atmosphere coupling via the soil moisture–boundary layer interaction, *J. Hydrometeorol.*, **12**, 766–786.
- Scheepmaker, R. A., C. Frankenberg, A. Galli, A. Butz, H. Schrijver, N. M. Deutsch, D. Wunch, T. Warneke, S. Fally, and I. Aben (2012), Improved water vapour spectroscopy in the 4174–4300cm<sup>-1</sup> region and its impact on sciamachy HDO/H<sub>2</sub>O measurements, *Atmos. Meas. Tech. Discuss.*, **5**, 8539–8578, doi:10.5194/amtd-5-8539-2012.
- Schlemmer, L., C. Hohenegger, J. Schmidli, C. Bretherton, and C. Schär (2011), An idealized cloud-resolving framework for the study of midlatitude diurnal convection over land, *J. Atmos. Sci.*, **68**, 1041–1057.
- Schlemmer, L., C. Hohenegger, J. Schmidli, and C. Schär (2012), Diurnal equilibrium convection and land surface-atmosphere interactions in an idealized cloud-resolving model, *Q. J. R. Meteorol. Soc.*, **138**(667), 1526–1539.
- Schmidt, G., G. Hoffmann, D. Shindell, and Y. Hu (2005), Modelling atmospheric stable water isotopes and the potential for constraining cloud processes and stratosphere-troposphere water exchange, *J. Geophys. Res.*, **110**, D21314, doi:10.1029/2005JD005790.
- Schneider, M., and F. Hase (2011), Optimal estimation of tropospheric H<sub>2</sub>O and deltaD with IASI/METOP, *Atmos. Chem. Phys.*, **11**, 11207–11220, doi:10.5194/acp-11-11207-2011.
- Schneider, M., G. Toon, J.-F. Blavier, F. Hase, and T. Leblanc (2010a), H<sub>2</sub>O and deltaD profiles remotely-sensed from ground in different spectral infrared regions, *Atmos. Meas. Tech.*, **3**, 1599–1613.
- Schneider, M., K. Yoshimura, F. Hase, and T. Blumenstock (2010b), The ground-based FTIR network's potential for investigating the atmospheric water cycle, *Atmos. Chem. Phys.*, **10**, 3427–3442.
- Schär, C., D. Lüthi, and U. Beyerle (1999), The soil-precipitation feedback: A process study with a regional climate model, *J. Clim.*, **12**, 722–741.
- Seneviratne, S. I., D. Lüthi, M. Litschi, and C. Schär (2006), Land-atmosphere coupling and climate change in Europe, *Nature*, **443**(14), 205–209, doi:10.1038/nature05095.
- Seneviratne, S. I., T. Corti, E. L. Davin, M. Hirschi, E. B. Jaeger, I. Lehner, B. Orlowsky, and A. J. Teuling (2010), Investigating soil moisture-climate interactions in a changing climate: A review, *Earth-Sci. Rev.*, **99**(3–4), 125–161, <http://dx.doi.org/10.1016/j.earscirev.2010.02.004>.
- Sitch, S. et al. (2003), Evaluation of ecosystem dynamics, plant geography and terrestrial carbon cycling in the LPJ dynamic vegetation model, *Global Change Biol.*, **9**, 161–185.
- Spracklen, D. V., S. R. Arnold, and C. M. Taylor (2012), Observations of increased tropical rainfall preceded by air passage over forests, *Nature*, **489**, 282–285, doi:10.1038/nature11390.
- Stewart, M. K. (1975), Stable isotope fractionation due to evaporation and isotopic exchange of falling waterdrops: Applications to atmospheric processes and evaporation of lakes, *J. Geophys. Res.*, **80**, 1133–1146.
- Taylor, C. M., and T. Lebel (1998), Observational evidence of persistent convective-scale rainfall patterns, *Mon. Weather Rev.*, **126**, 1597–1607, <http://dx.doi.org/10.1175/1520-0493>.
- Taylor, C. M., D. J. Parker, and P. P. Harris (2007), An observational case study of mesoscale atmospheric circulations induced by soil moisture, *Geophys. Res. Lett.*, **34**, L15801, doi:10.1029/2007GL030572.
- Taylor, C. M., P. P. Harris, and D. J. Parker (2009), Impact of soil moisture on the development of a Sahelian mesoscale convective system: a case study from the AMMA special observing period, *Q. J. R. Meteorol. Soc.*, **136**, 456–470, doi:10.1002/qj.465.
- Taylor, C. M., A. Gounou, F. Guichard, P. P. Harris, R. J. Ellis, F. Couvreux, and M. De Kauwe (2011), Frequency of Sahelian storm initiation enhanced over mesoscale soil-moisture patterns, *Nat. Geosci.*, **4**, 430–433.
- Taylor, C. M., R. A. M. de Jeu, F. Guichard, P. P. Harris, and W. A. Dorigo (2012), Afternoon rain more likely over drier soils, *Nature*, **489**, 423–426, doi:10.1038/nature11377.
- Tindall, J. C., P. Valdes, and L. C. Sime (2009), Stable water isotopes in HadCM3: Isotopic signature of El Niño-Southern Oscillation and the tropical amount effect, *J. Geophys. Res.*, **114**, D04111, doi:10.1029/2008JD010825.
- Tremoy, G., F. Vimeux, S. Mayaki, I. Souley, O. Cattani, G. Favreau, and M. Oi (2012), A 1-year long delta18O record of water vapor in Niamey (Niger) reveals insightful atmospheric processes at different timescales, *Geophys. Res. Lett.*, **39**, L08805, doi:10.1029/2012GL051298.
- Trenberth, K. (1999), Atmospheric moisture recycling: Role of advection and local evaporation, *J. Clim.*, **12**, 1368–1381.
- Tuinenburg, O. A., R. W. A. Hutjes, C. M. J. Jacobs, and P. Kabat (2011), Diagnosis of local land–atmosphere feedbacks in India, *J. Clim.*, **24**, 251–266, doi:10.1175/2010JCLI3779.1.
- Uppala, S., et al. (2005), The ERA-40 re-analysis, *Q. J. R. Meteorol. Soc.*, **131**, 2961–3012.
- van der Ent, R. J., H. H. G. Savenje, B. Schaeffli, and S. C. Steele-Dunne (2010), Origin and fate of atmospheric moisture over continents, *Water Resour. Res.*, **46**, 1853–1863, doi:10.5194/acp-11-1853-2011.
- van der Ent, R. J., and H. H. G. Savenje (2011), Length and time scales of atmospheric moisture recycling, *Atmos. Chem. Phys.*, **11**, 1853–1863, doi:10.5194/acp-11-1853-2011.
- Vimeux, F., R. Gallaire, S. Bony, G. Hoffmann, and J. C. H. Chiang (2005), What are the climate controls on deltaD in precipitation in the Zongo Valley (Bolivia)? Implications for the Illimani ice core interpretation, *Earth Planet. Sci. Lett.*, **240**, 205–220.
- Vimeux, F., G. Tremoy, C. Risi, and R. Gallaire (2011), A strong control of the South American SeeSaw on the intraseasonal variability of the isotopic composition of precipitation in the Bolivian Andes, *Earth Planet. Sci. Lett.*, **307**(1–2), 47–58.
- Washburn, E., and E. Smith (1934), The isotopic fractionation of water by physiological processes, *Science*, **79**, 188–189.
- Wei, J., and P. A. Dirmeyer (2010), Toward understanding the large-scale land-atmosphere coupling in the models: roles of different processes, *Geophys. Res. Lett.*, **37**, L19797, doi:10.1029/2010GL044769.
- Welp, L., W. Lee, T. J. Griffis, X.-F. Wen, W. Xiao, S. Li, X. Sun, Z. Hu, M. Val Martin, and J. Huang (2012), A meta-analysis of water vapor deuterium-excess in the midlatitude atmospheric surface layer, *Global Biogeochem. Cycles*, **26**, GB3021, doi:10.1029/2011GB004246.
- Werner, M., P. M. Langebroek, T. Carlsen, M. Herold, and G. Lohmann (2011), Stable water isotopes in the ECHAM5 general circulation model: Toward high-resolution isotope modeling on a global scale, *J. Geophys. Res.*, **116**, D15109, doi:10.1029/2011JD015681.
- Westra, D., G. J. Steeneveld, and A. A. M. Holtslag (2012), Some observational evidence for dry soils supporting enhanced high relative humidity at the convective boundary layer top, *J. Hydrometeorol.*, **13**, 1347–1358.
- Worden, J., et al. (2006), Tropospheric emission spectrometer observations of the tropospheric HDO/H<sub>2</sub>O ratio: Estimation approach and characterization, *J. Geophys. Res.*, **111**, D16309, doi:10.1029/2005JD006606.
- Worden, J., D. Noone, and K. Bowman (2007), Importance of rain evaporation and continental convection in the tropical water cycle, *Nature*, **445**, 528–532.
- Worden, J., D. Noone, J. Galewsky, A. Bailey, K. Bowman, D. Brown, J. Hurley, S. Kulawik, J. Lee, and M. Strong (2010), Estimate of bias in Aura TES HDO/H<sub>2</sub>O profiles from comparison of TES and in situ HDO/H<sub>2</sub>O measurements at the Mauna Loa Observatory, *Atmos. Chem. Phys. Discuss.*, **10**, 25355–25388, doi:10.5194/acpd-10-25355-2010.
- Worden, J., S. Kulawik, C. Frankenberg, K. Bowman, V. Payne, K. Cady-Peirara, K. Wecht, J.-E. Lee, and D. Noone (2012a), Profiles of CH<sub>4</sub>, HDO, H<sub>2</sub>O, and N<sub>2</sub>O with improved lower tropospheric vertical resolution from Aura TES radiances, *Atmos. Meas. Tech. Discuss.*, **5**, 397–411, doi:10.5194/amtd-5-397-2012.
- Worden, J., K. Wecht, C. Frankenberg, M. Alvarado, K. Bowman, E. Kort, S. Kulawik, M. Lee, V. Payne, and H. Worden (2012b), CH<sub>4</sub> and CO distributions over tropical fires as observed by the Aura TES satellite instrument and modeled by GEOS-Chem, *Atmos. Chem. Phys. Discuss.*, **12**, 26207–26243.
- Wunch, D., G. C. Toon, J.-F. L. Blavier, R. A. Washenfelder, J. Notholt, B. J. Connor, D. W. T. Griffith, V. Sherlock, and P. O. Wennberg (2011), The total carbon column observing network, *Phil. Trans. R. Soc. A*, **369**(1943), 2087–2112, doi:10.1098/rsta.2010.0240.

- Yoshimura, K., C. Frankenberg, J. Lee, M. Kanimatsu, J. Worden, and T. Rockmann (2001), Comparison of an isotopic atmospheric general circulation model with new quasi-global satellite measurements of water vapor isotopologues, *J. Geophys. Res.*, *116*:D19118, doi:10.1029/2011JD016035.
- Yoshimura, K., T. Oki, N. Ohte, and S. Kanae (2004), Colored moisture analysis estimates of variations in 1998 Asian monsoon water sources, *J. Meteorol. Soc. Japan*, *82*, 1315–1329.
- Yoshimura, K., M. Kanamitsu, D. Noone, and T. Oki (2008), Historical isotope simulation using reanalysis atmospheric data, *J. Geophys. Res.*, *113*, D19108, doi:10.1029/2008JD010074.
- Zaitchik, B. F., A. K. Macalady, L. R. Bonneau, and R. B. Smith (2006), Europe's 2003 heat wave: A satellite view of impacts and land-atmosphere feedbacks, *Int. J. Climatol.*, *26*(6), 743–769.
- Zangvil, A., D. H. Portis, and P. J. Lamb (2004), Investigation of the large-scale atmospheric moisture field over the midwestern United States in relation to summer precipitation. Part II: Recycling of local evapotranspiration and association with soil moisture and crop yields, *J. Clim.*, *17*, 3283–3301.
- Zipser, E., and M. A. LeMone (1980), Cumulonimbus vertical velocity events in gate. Part II: Synthesis and model core structure, *J. Atmos. Sci.*, *37*, 2458–2469.